decreased at 24 HAT, and then returned to the control level at 48 HAT. TUNEL-positive cells in the fetal brains of control and VP-16-treated fetal mice were cited in a previous study [28]. The number of TUNEL-positive cells increased significantly from 8 HAT, reached a peak at 12 HAT, decreased at 24 HAT, and then returned to the control level at 48 HAT.

3.2. Immunohistochemistrical findings

In the brains of fetuses obtained from dams treated with VP-16 on GD12, p53- and p21-positive neuroepithelial cells were observed in the telencephalons.

Changes in the number of p53-positive neuroepithelial cells are shown in Fig. 1. Few p53-positive neuroepithelial cells were observed in the ventricular zone (VZ) of the telencephalic wall of control fetuses. In VP-16-exposed fetuses, however, p53-positive cells increased remarkably in the VZ of the telencephalic wall. The number of p53-positive neuroepithelial cells of VP-treated fetuses began to increase significantly from 2 HAT, reached a peak at 4 HAT, decreased gradually at 8 HAT, and then returned to the control level at 48 HAT.

Changes in the number of p21-positive cells are shown in Fig. 2. Few p21-positive neuroepithelial cells were observed in the VZ of the telencephalic wall of control fetuses. The number of p21-positive neuroepithelial cells of VP-16-exposed fetuses reached a peak at 4 HAT, decreased gradually at 8 HAT, and then returned to the control level at 48 HAT. In VP-16-treated fetuses, the increase of the number of p21-positive cells was less prominent than that of p53-positive cells.

3.3. Findings of RT-PCR

Results of semi-quantitative RT-PCR are shown in Figs. 3 and 4. The expression of *p21*, *fas*, and *puma* mRNAs increased significantly in VP-16-exposed fetuses. The expression of *p21* mRNA reached a peak at 4 HAT, decreased at 8 HAT, and then returned to the control level at 12 HAT. The expression of *fas* mRNA began to increase at 2 HAT, peaked at 8 HAT, decreased at 12 HAT, and then returned to control level at the 24 HAT. The expression of *puma* mRNA increased significantly throughout the experimental period. On the other hand, the expression of *p53*, *bax*, and *cyclin G1* mRNA did not change significantly throughout the experimental period.

3.4. Cell cycle analysis

Results of flow cytometric analysis are shown in Fig. 5. The sub-G1 fraction (apoptotic cells) of VP-16-exposed fetuses began to increase significantly at 4 HAT, peaked at 12 HAT, decreased gradually at 24 HAT, and then returned to the control level at 48 HAT. The S and G2/M fractions also increased significantly at 4 and 8 HAT with VP-16.

3.5. Migration of neuroepithelial cells

BrdU-injection caused no significant histopathological changes in the control fetuses. The migration of BrdU-positive neuroepithelial cells in the telencephalic wall is showna in Fig. 6.

In control fetuses, BrdU-positive cells were seen mainly in the dorsal layer (DL) and partly in the medial layer (ML) at 1 and 2 HAT. At 4 HAT, BrdU-positive cells in the ventricular layer (VL) increased, while the cells in the DL decreased. At 8 HAT, most of BrdU-positive cells were observed in the VL and ML. At 12 HAT, BrdU-positive cells were prominently observed again in the DL and ML, while few BrdU-positive cells were observed in the VL. At 24 HAT, BrdU-positive cells were rarely observed in the DL, ML or VL. Some BrdU-positive cells were seen in the superficial layer from 4 HAT and 24 HAT. Therefore, BrdU was incorporated mainly into neuroepithelial cells in the DL until 1 HAT, and the cells migrated through the ML to VL, and divided along the lateral ventricle from 4 HAT to 8 HAT. The cells retuned to the DL through the ML from 8 HAT to 12 HAT.

In the VP-16-exposed fetuses, BrdU-positive cells were also seen mainly in the DL and partly in the ML at 1 and 2 HAT. At this time, the number of mitotic cells in the VZ was significantly decreased as compared to that in the control (data not shown) [28]. At 8 HAT, BrdU-positive cells were mainly seen in the VL and partly in the ML. At 12 HAT, BrdU-positive cells were observed mainly in the ML, and partly in the DL. At 24 HAT,

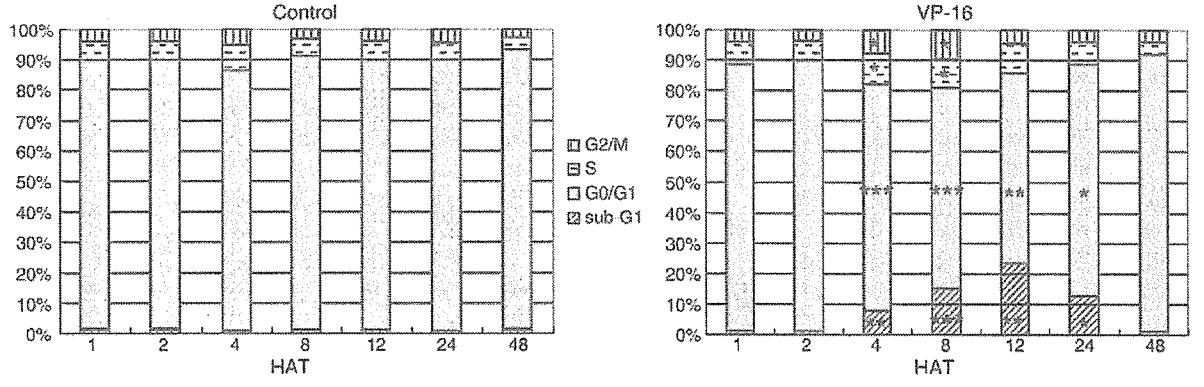

Fig. 5. Percentage of cells in each cell cycle phase. VP-16 induces S-phase accumulation and G2-M cell arrest as well as apoptosis. Percentages for each cell cycle presents as the mean of three fetuses from each dam. $^{*}p<0.05$, $^{**}p<0.01$, $^{***}p<0.001$: significantly different from controls by Student's *t* test.

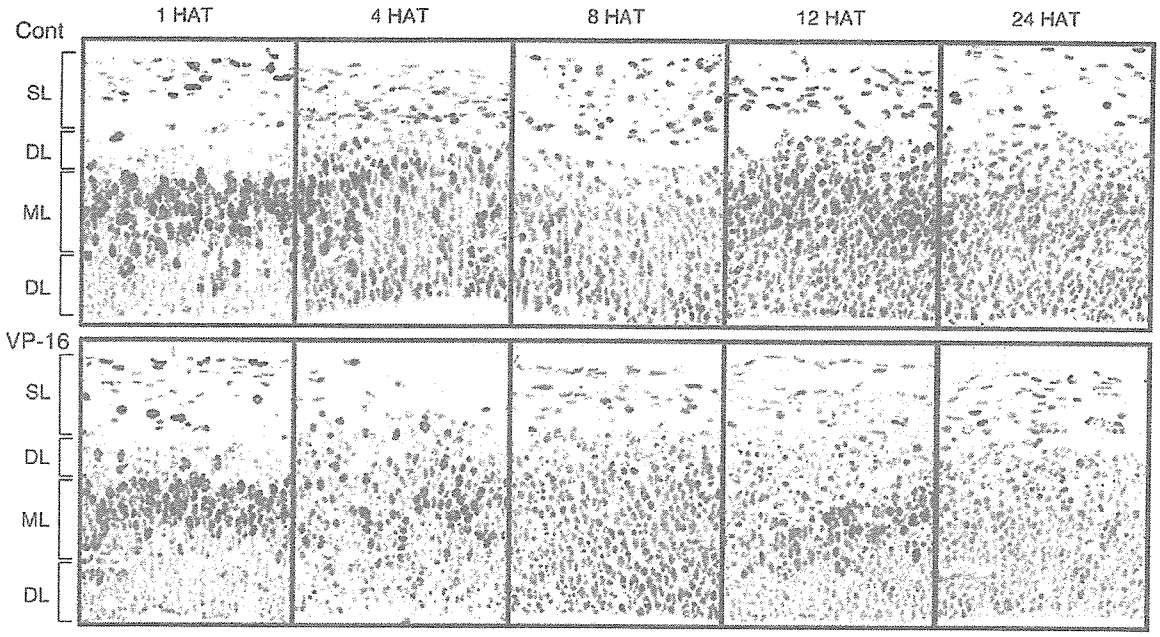

Fig. 6. Migration of BrdU-positive cells in the telencephalic wall. BrdU was administered simultaneously with VP-16 or vehicle. ×200.

BrdU-positive cells were rarely observed in the DL, ML or VL. Pyknotic cells were observed from 4 to 24 HAT, and BrdU-positive signals were also detected in some pyknotic cells from 8 to 12 HAT.

4. Discussion

Embryos and fetuses are very sensitive to DNA damage such as that caused by radiation, and DNA-damaging chemicals, which induce congenital anomalies [1,22,33,35,39]. DNA-damaging teratogens induce excessive apoptosis by the p53-dependent pathway [18,21,42,44]. p53 is also reported to be a suppressor of teratological insults [29,30]. p53-deficient mice are more susceptibile to DNA-damaging teratogens, resulting in increased embryonic death and birth defects [21,26,29,30]. These studies suggested that absence of p53 might decrease DNA repair and accumulate DNA damage in response to the teratogens. Although accumulation of DNA damage in p53-lacking embryos causes severe developmental anomalies, excessive p53-dependent apoptosis in normal mice also causes moderate malformations [26]. However, it is obvious that p53 plays a crucial role in causing cell cycle arrest, apoptosis and repair, in response to DNA-damaging teratogens.

The present study clarified that VP-16-administraion to pregnant mice caused 1) increases of p53 and p21 proteins, 2) increases of mRNA expression of p53 target genes, such as *p21*, *fas* and *puma*, and 3) apoptosis, S-phase accumulation, and G2/M arrest in the fetal brain.

Although the mRNA expression of *p53* was not increased by VP-16 treatment, the number of p53-positive cells was increased markedly compared to that in the controls. It is known that DNA-damaging agents stabilize p53 protein and increase the phosphorylation of p53 [4,5]. The increase of p53 protein by VP-16 treatment was detected prior to the induction of cell cycle arrest and apoptosis in the fetal telencephalon.

The expression of *p21* mRNA and protein also increased in the fetal brain after VP-16 administration. p21, a cyclin-dependent kinase 2 inhibitor, induces cell cycle arrest at G1 phase [9], and also causes partially to G2/M arrest through inhibition of the G2/M regulatory cyclin B1-Cdc2 complex *in vitro* [13,14]. Despite the p21-upregulation, the exposure to 4 mg/kg VP-16 caused only S-phase accumulation and G2/M arrest, not G1 arrest, in the fetal brain. Furthermore, VP-16 treatment of embryonic fibroblasts of *p53*-deficient mice led to S and G2/M arrest *in vitro* [3]. Moreover, VP-16 treatment could also activate p21 through an ATM-ERK-pathway, not the p53-dependent pathway, *in vitro* [41]. It is therefore supposed that p53 may not play a crucial role in the induction of cell cycle arrest by VP-16 treatment. p21 may instead may protect cells from DNA damage by binding to Rad51 and enhancing the repair of DNA damage [36]. Thus, the precise role of p53-dependent p21 upregulation in the cell cycle arrest induced in the mouse fetal brain by VP-16 is still unclear, and further studies will be necessary to clarify the role of p21.

The mRNA expression of *fas* and *puma* was increased markedly by VP-16 administration. Fas is a membrane protein and a death receptor which belongs to the tumor necrosis factor receptor family [15], and induces apoptosis when it binds to fas ligand [27]. Puma is directly induced by p53 in response to DNA damage [45]. It is clear that VP-16-induced apoptosis might involve both extrinsic and intrinsic apoptosis pathways. On the other hand, the expression of *bax* mRNA was not increased by VP-16 administration. Puma promotes mitochondrial translocation and multimerization of *bax* [46], which is curious because the expression of *bax* mRNA was not increased despite the upregulation of *puma* mRNA by VP-16 administraion. Further

studies of protein expression, including Puma and bax expression, will be required to elucidate the apoptotic mechanism.

In a previous study [28], we reported that apoptosis of neuroepithelial cells in the central nervous system was induced by VP-16 administration to pregnant mice on GD12. The number of mitotic neuroepithelial cells was decreased significantly at 2 and 4 HAT. Pyknotic neuroepithelial cells were observed from 4 to 24 HAT. The number of TUNEL-positive cells began to increase significantly from 8 HAT, peaked at 12 HAT, decreased at 24 HAT, and then returned to the control level at 48 HAT.

In BrdU-immunostaining study, a delay of the migration of neuroepithelial cells in the fetal telencephalon was detected after VP-16-injection into dams. BrdU-immunostaining revealed BrdU-positive signals in some pyknotic cells. It is known that most of BrdU-positive cells are S phase cells. Mitotic neuroepithelial cells prominently decreased at 2 and 4 HAT. From these results, it was supposed that VP16 exposure on fetal mice might damage S phase cells and alter the cell cycle of neuroepithelial cells. In addition, the pattern of distribution of BrdU-positive cells seen in the DL and ML at 1 HAT appeared again at 12 HAT, implying that the proliferative cycle of neuroepithelial cells in E12.5 is about 12 h s long.

In cell cycle analysis, the increase of sub-G1 cells was in accord with the sequential increase of pyknotic cells and TUNEL-positive cells after VP-16 treatment. Also, S phase accumulation and G2/M cell cycle arrest was significantly increased at 4 HAT and 8 HAT. Based on these results, we suggest that VP-16 might induce S and G2/M arrest through its toxic effects on S and G2 phase cells, and may the inhibit G2/M transition of neuroepithelial cells in the fetal brain.

In conclusion, the data obtained in this study demonstrated that VP-16 induced apoptosis and G2/M cell cycle arrest through a p53-related pathway in the mouse fetal brain when dams were exposed to VP-16 on GD12.

References

[1] B.P. Adlard, J. Dobbing, J. Sandas, A comparison of the effects cytosine arabinoside and adenine arabinoside on some aspects of brain growth and development in the rat, Br. J. Pharmacol. 54 (1975) 33–39.

[2] E. Appella, C.W. Anderson, Post-translational modifications and activation of p53 by genotoxic stresses, Eur. J. Biochem. 268 (2001) 2764–2772.

[3] L.D. Attardi, A. de-Vries, T. Jacks, Activation of p53-dependent G1 checkpoint response in mouse embryo fibroblast depends on the specific DNA damage inducer, Oncogene 23 (2004) 973–980.

[4] S. Banin, L. Moyal, S. Shieh, Y. Taya, C.W. Anderson, L. Chessa, N.I. Smorodinsky, C. Prives, Y. Reiss, Y. Shiloh, Y. Ziv, Enhanced phosphorylation of p53 by ATM in response to DNA damage, Science 281 (1998) 1674–1677.

[5] C.E. Canman, D.S. Lim, K.A. Cimprich, Y. Taya, K. Tamai, K. Sakaguchi, E. Appella, M.B. Kastan, J.D. Siliciano, Activation of the ATM kinase by ionizing radiation and phosphorylation of p53, Science 281 (1998) 1677–1679.

[6] A.Y. Chen, L.F. Liu, DNA topoisomerases: essential enzymes and lethal targets, Annu. Rev. Pharmacol. Toxicol. 34 (1994) 191–218.

[7] C. Culmsee, M.P. Mattson, p53 in neuronal apoptosis, Biochem. Biophys. Res. Commun. 331 (2005) 761–777.

[8] W.S. el-Diery, T. Tokino, V.E. Velculescu, D.B. Levy, R. Parsons, J.M. Trent, D. Lin, W.E. Mercer, K.W. Kinzler, B. Vogelstein, WAF1, a potential mediator of p53 tumor suppression, Cell 75 (1993) 817–825.

[9] W.S. el-Deiry, J.W. Harper, P.M. O'Connor, V.E. Velculescu, C.E. Canman, J. Jackman, J.A. Pietenpol, M. Burrell, D.E. Hill, Y. Wang, WAF1/CIP1 is induced in p53-mediated G1 arrest and apoptosis, Cancer Res. 54 (1994) 169–1174.

[10] T.G. Gantchev, D.J. Hunting, Enhancement of etoposide (VP-16) cytotoxicity by enzymatic and photodynamically induced oxidative stress, Anticancer Drugs 8 (1997) 164–173.

[11] K.R. Hande, Etoposide: four decades of development of topoisomerase II inhibitor, Eur. J. Cancer 34 (1998) 1514–1521.

[12] J.W. Harper, S.J. Elledges, K. Keyomarsi, B. Dynlacht, L.H. Tsai, P. Zhang, S. Dobrowolski, C. Bai, L. Connell-Crowley, E. Swindell, M.P. Fox, N. Wei, Inhibition of cyclin-dependent kinases by p21, Mol. Biol. Cell 6 (1995) 387–400.

[13] S. Haupt, M. Berger, Z. Goldberg, Y. Haupt, Apoptosis — the p53 network, J. Cell Sci. 116 (2003) 4077–4085.

[14] S.A. Innocents, J.L. Abrahamson, J.P. Cogswell, J.M. Lee, p53 regulates a G_2 checkpoint through cyclin B1, Proc. Natl. Acad. Sci. U. S. A. 96 (1999) 2147–2152.

[15] N. Itoh, S. Yonehara, A. Ishii, M. Yonehara, S. Mizushima, M. Sameshima, A. Hase, Y. Seto, S. Nagata, The polypeptide encoded by the cDNA for human cell surface antigen fas can mediate apoptosis, Cell 66 (1991) 233–243.

[16] J.R. Jeffers, E. Parganas, Y. Lee, C. Yang, J. Wang, J. Brennan, K.H. MacLean, J. Han, T. Chittenden, J.N. Ihle, P.J. McKinnon, J.L. Cleveland, G.P. Zambetti, *PUMA* is an essential mediator of p53-dependent and -independent apoptotic pathway, Cancer Cell 4 (2003) 321–328.

[17] M.B. Kastan, Q. Zhan, W.S. el-Diery, F. Carrier, T. Jacks, W.V. Walsh, B.S. Plunkett, B. Vogelstein, A.J. Fornance, A mammalian cell cycle checkpoint pathway utilizing p53 and *GADD45* is defective in ataxia–telengiectasia, Cell 171 (1992) 587–597.

[18] K. Katayama, M. Ueno, H. Yamauchi, T. Nagata, H. Nakayama, K. Doi, Ethylnitrosourea induces neural progenitor cell apoptosis after S-phase accumulation in a p53-dependent manner, Neurobiol. Dis. 18 (2005) 218–225.

[19] S.H. Kimura, H. Nojima, Cyclin G1 associates with mdm2 and regulates accumulation and degradation of *p53* protein, Genes Cells 7 (2002) 869–880.

[20] L.J. Ko, C. Prives, p53: puzzle and paradigm, Genes Dev. 10 (1996) 1054–1072.

[21] Y. Kubota, S. Takahashi, X.Z. Sun, H. Sato, S. Aizawa, K. Yoshida, Radiation-induced tissue abnormalities in fetal brain are related to apoptosis immediately after irradiation, Int. J. Radiat. Biol. 76 (2000) 649–659.

[22] J. Langman, M. Shimada, Cerebral cortex of the mouse after prenatal chemical insult, Am. J. Anat. 132 (1971) 355–374.

[23] A.J. Levine, p53, the cellular gatekeeper for growth and division, Cell 88 (1997) 323–331.

[24] R. Li, S. Waga, G.J. Hannon, D. Beach, B. Stillmann, Differential effects by the p21 CDK inhibitor on PCNA-dependent DNA replication and repair, Nature 371 (1994) 534–537.

[25] E.R. McDonald III, G.S. Wu, T. Waldman, W.S. el-Diery, Repair defect in p21WAP1/CIP1−/− human cancer cells, Cancer Res. 56 (1996) 2250–2255.

[26] S.A. Moallem, B.F. Hales, The role of p53 and cell death by apoptosis and necrosis in 4-hydroperoxycyclophosphamide-induced limb malformations, Development 125 (1998) 3225–3234.

[27] M. Muller, S. Wilder, D. Bannasch, D. Israeli, K. Lelhbach, M. Li-Weber, S.L. Freiderman, P.R. Galle, W. Stremmel, M. Oren, P.H. Krammer, p53 activates the CD95 (APO-1/fas) gene in response to DNA damage by anticancer drugs, J. Exp. Med. 188 (1998) 2033–2045.

[28] C. Nam, G.H. Woo, K. Uetsuka, H. Nakayama, K. Doi, Histopathological changes in the brain of mouse fetuses by etoposide administration, Histol. Histopathol. 21 (2006) 257–263.

[29] C.J. Nicol, M.L. Harrison, P.R. Laposa, I.L. Gimelshtein, P.G. Wells, A teratological suppressor role for p53 in benzo[a]pyrene-treated transgenic *p53*-deficient mice, Nat. Genet. 10 (1995) 181–187.

[30] T. Norimura, S. Nomoto, M. Katsuki, Y. Gondo, S. Kondo, p53-dependent apoptosis suppresses radiation-induced teratogenesis, Nat. Med. 2 (1996) 577–580.

[31] E. Oda, R. Ohki, H. Murasawa, J. Nemoto, T. Shibue, T. Yamashita, T. Tokino, T. Taniguchi, N. Tanaka, Noxa, a BH3-only member of the Bcl-2

family and candidate mediator of p53-induced apoptosis, Science 288 (2000) 1053–1058.
[32] K. Okamoto, D. Beach, Cyclin G is a transcriptional target of the *p53* tumor suppressor protein, EMBO J. 13 (1994) 4816–4822.
[33] E. Ozu, Effects of low-dose x-irradiation on early mouse embryos, Radiat. Res. 26 (1965) 107–113.
[34] Z.Q. Pan, J.T. Readorn, L. Li, H. Flores-Rozas, R. Legerski, A. Sancar, J. Hurwitz, Inhibition of nucleotide excision repaired by the cyclin-dependent kinase inhibitor of p21, J. Biol. Chem. 270 (1995) 22008–22016.
[35] M.J. Pfafferenorth, G.D. Das, J.P. McAllister, Teratologic effects of ethylnitrosourea on brain development in rats, Teratology 9 (1974) 305–315.
[36] E. Radershall, A. Bazarov, J. Cao, R. Lurz, A. Smith, W. Mann, H. Ropers, J.M. Sedivy, E.I. Golub, E. Fritz, T. Haaf, Formation of higher-order nuclear Rad51 structure is functionally linked to *p21* expression and protection from DNA damage-induced apoptosis, J. Cell Sci. 115 (2002) 153–164.
[37] M.J. Robinson, N. Oscheroff, Effects of antineoplastic drugs on the post-strand-passage DNA cleavage/religation equilibrium of topoisomerase II, Biochemistry 30 (1991) 1807–1813.
[38] M. Selvakumaran, H.K. Lin, T. Miyashita, H.G. Wang, S. Krajewski, J.C. Reed, B. Hoffmann, D. Liebermann, Immediate early up-regulation of *bax* expression by p53 but not TGF beta 1: a paradigm for distinct apoptotic pathways, Oncogene 9 (1994) 1791–1798.
[39] S.M. Sieber, J. Whang-Peng, C. Botkin, T. Knutsen, Teratogenic and cytogenetic effects of some plant-derived antitumor agents (vincristine, colochicine, maytasine, VP-16-213 and VM-216) in mice, Teratology 18 (1978) 31–48.
[40] Z.A. Stewart, J.A. Pietenpol, p53 signaling and cell cycle checkpoints, Chem. Res. Toxicol. 14 (3) (2001) 243–263.
[41] D. Tang, D. Wu, A. Hirao, J.M. Lahti, L. Liu, B. Mazza, V.J. Kidd, T.W. Mak, A.J. Ingram, ERK activation mediates cell cycle arrest and apoptosis after DNA damage Independently of p53, J. Biol. Chem. 277 (2002) 12710–12717.
[42] M. Ueno, K. Katayama, H. Nakayama, K. Doi, Mechanisms of 5-azacytidine (5AzC)-induced toxicity in the rat foetal brain, Int. J. Exp. Pathol. 83 (2002) 139–150.
[43] B. Vogelstein, D. Lane, A.J. Levine, Surfing the p53 network, Nature 408 (2000) 307–310.
[44] H. Yamauchi, K. Katayama, M. Ueno, K. Uetsuka, H. Nakayama, K. Doi, Involvement of p53 in 1-beta-D-arabinofuranosylcytosine-induced rat fetal brain lesions, Neurotoxicol. Teratol. 26 (4) (2004) 579–586.
[45] J. Yu, L. Zhang, P. Hwang, K.W. Kinzler, B. Vogelstein, *PUMA* induces the rapid apoptosis of colorectal cancer cells, Mol. Cell 7 (2001) 673–682.
[46] J. Yu, Z. Wang, K.W. Kinzler, B. Vogelstein, L. Zhang, *PUMA* mediates the apoptotic response to p53 in colorectal cancer cells, Proc. Natl. Acad. Sci. U. S. A. 100 (2003) 1931–1936.

Human Vascular Smooth Muscle Cells Express a Urate Transporter

Karen L. Price,*† Yuri Y. Sautin,* David A. Long,*‡ Li Zhang,* Hiroki Miyazaki,§ Wei Mu,* Hitoshi Endou,§ and Richard J. Johnson*

*Division of Nephrology, Hypertension, and Transplantation, University of Florida, Gainesville, Florida; †Institute of Urology and Nephrology and ‡Nephro-Urology Unit, Institute of Child Health, University College London, United Kingdom; and §Department of Pharmacology and Toxicology, Kyorin University School of Medicine, Tokyo, Japan

An elevated serum uric acid is associated with the development of hypertension and renal disease. Renal regulation of urate excretion is largely controlled by URAT1 (*SLC22A12*), a member of the organic anion transporter superfamily. This study reports the specific expression of URAT1 on human aortic vascular smooth muscle cells, as assessed by reverse transcription–PCR and Western blot analysis. Expression of URAT1 was localized to the cell membrane. Evidence that the URAT1 transporter was functional was provided by the finding that uptake of ^{14}C-urate was significantly inhibited in the presence of probenecid, an organic anion transporter inhibitor. It is proposed that URAT1 may provide a mechanism by which uric acid enters the human vascular smooth muscle cell, a finding that may be relevant to the role of uric acid in cardiovascular disease.

J Am Soc Nephrol 17: 1791–1795, 2006. doi: 10.1681/ASN.2006030264

Urate is generated as a result of purine metabolism. In most species, this is an intermediate product that is degraded further by the hepatic enzyme uricase to allantoin, which then is excreted freely in the urine (1). In humans, however, urate is the final breakdown product as a result of a mutation that renders the uricase gene nonfunctional (2); as a consequence, humans have higher serum urate levels (>2 mg/dl) compared with most mammals (<2 mg/dl) (1).

Hyperuricemia, usually defined as >7 mg/dl in men and >6 mg/dl in women (1), has been identified as a risk factor in the development of hypertension and renal disease (3–6). We showed previously that raising uric acid in rats *via* the administration of an uricase inhibitor leads to a thickening of the afferent arteriole, endothelial dysfunction, activation of the renin-angiotensin system, and hypertension (7–11). Similarly, uric acid stimulates rat vascular smooth muscle cell (VSMC) proliferation *in vitro* with increased expression of platelet-derived growth factor (PDGF), cyclooxygenase-2, and monocyte chemoattractant protein-1 (12,13). Uric acid also stimulates human VSMC proliferation and synthesis of C-reactive protein (CRP) (14).

These observations raise the question of how uric acid enters the VSMC and the transporters involved. In the kidney, uric acid is reabsorbed and secreted primarily by the organic anion transporter (OAT) superfamily, which consists of OAT1 (*SLC22A6*) (15), OAT2 (*SLC22A7*) (16), OAT3 (*SLC22A8*) (17), OAT4 (*SLC22A9*) (18), and the recently cloned URAT1 (*SLC22A12*) (19). The expression of these transporters has been investigated in proximal tubular epithelial cells (20) and rat VSMC (21). With regard to human VSMC, we previously reported that probenecid (an organic anion transport inhibitor) can significantly inhibit uric acid–induced proliferation and C-reactive protein expression (14). Therefore, we hypothesized that the human VSMC may express an OAT similar to that expressed in the proximal tubular cell. We demonstrate that URAT1 may be the transporter by which uric acid enters human VSMC.

Methods and Materials

Cell Culture

Human aortic VSMC were obtained from Prof. Elaine Raines (University of Washington, Seattle, WA) and cultured as described previously (22). Briefly, cells were cultured in DMEM (Invitrogen, Carlsbad, CA) supplemented with 20% FBS (Invitrogen), 25 mM HEPES (Invitrogen), 100 U/ml penicillin, and 100 mg/ml streptomycin (Invitrogen). Cells were subcultured 1:3 on confluence. All experiments were performed on at least three independent occasions with cells between passages 4 and 8.

Uric Acid Stimulation

Cells were grown to 70% confluence, serum-starved 24 h before experimentation and challenged with varying concentrations of uric acid (3 to 12 mg/dl) for 6 h to collect RNA and 24 h to collect protein. In addition, RNA and protein were collected from nonstimulated cells at the same time points for comparison.

Reverse Transcription–PCR Amplification

RNA was isolated using Tri-Reagent (Sigma, St. Louis, MO) and extracted with isopropanol (Sigma) followed by ethanol precipitation. One microgram of RNA was used to create cDNA, according to providers' instructions (Bio-Rad Laboratories, Hercules, CA). Two micro-

Published online ahead of print. Publication date available at www.jasn.org.

Address correspondence to: Dr. Karen L. Price, Institute of Urology and Nephrology, University College London, 67 Riding House Street, London W1W 7EJ, UK. Phone: +44-20-7679-9113; Fax: +44-20-7679-9296; E-mail: regnkpr@ucl.ac.uk

ISSN: 1046-6673/1707-1791

liters of cDNA product was used in a 50-μl final volume reaction that contained 1.5 mM $MgCl_2$, 200 μl dNTP, iTaq buffer (200 mM Tris-HCl [pH 8.4] and 500 mM KCl), 100 nM of both sense and antisense primers, and 1.25 U of iTaq DNA polymerase (Bio-Rad Laboratories). cDNA preparations from human kidney, human liver, and human placenta poly A^+ RNA (Clontech, San Jose, CA) were used as positive controls for the appropriate gene: human kidney for OAT1, OAT3, and URAT1 (15,17,19); human liver for OAT2 (16); and human placenta for OAT4 (18). A negative control that consisted of the PCR mixture excluding template cDNA was included. The PCR primers and conditions used are shown in Table 1. Results shown are representative agarose gels of at least three independent experiments. In addition, the identity of the PCR products produced was confirmed by forward and reverse sequence analysis (Sigma Genosys, The Woodlands, TX).

Western Blot Analysis for URAT1

Cells were lysed in RIPA buffer (150 mM NaCl, 1% Nonidet P-40, 0.5% sodium deoxycholate, 0.1% SDS, and 50 mM Tris buffer [pH 8.0]), and Western blotting was performed using 15 μg of protein as described previously (23). Briefly, after electrophoresis and transfer by electroblotting, membranes were blocked in 5% nonfat milk for 1 h before incubation with rabbit anti-human URAT1 (1:500; Alpha Diagnostic Inc., San Antonio, TX) overnight at 4°C. Appropriate horseradish peroxidase antibodies (DAKO, Carpinteria, CA) were then used, and bands were detected by chemiluminescence (Amersham Biosciences, Piscataway, NJ). Blots were stripped and reprobed with human glyceraldehyde-3-phosphate dehydrogenase (1:300; Chemicon International, Temecula, CA), to assess equal loading. The result of the Western blot shown is representative of at least three independent experiments.

Total Membrane Isolation

Human VSMC that were grown to 70% confluence were washed three times with ice-cold Krebs Ringer Buffer (128 mM NaCl, 4.7 mM KCl, 1.25 mM $MgSO_4 \cdot 7H_2O$, 1.25 mM $CaCl_2 \cdot 2H_20$, and 5 mM phosphate salts), collected in Buffer A (20 mM Tris-HCl, 1 mM EDTA, and 255 mM sucrose [pH 7.4]) that contained protease inhibitors, homogenized on ice, and centrifuged at 55,000 rpm for 70 min at 4°C. The cell pellet was resuspended in 200 μl of Buffer A, and the protein concentration was determined. A total of 80 μg of protein was used as described above for Western blot analysis. The result of the Western blot shown is representative of at least three independent experiments.

Immunolocalization of URAT1 on VSMC

To confirm membrane localization of URAT1, we performed indirect immunofluorescence staining. VSMC were fixed in 3% paraformaldehyde, quenched in 50 mM ammonium chloride and treated with 0.1% Triton X-100 for 10 min. Cells then were incubated overnight at 4°C using an anti-human URAT1 N-terminal polyclonal antibody followed by a donkey anti-rabbit antibody conjugated to Texas Red (Jackson ImmunoResearch, West Grove, PA) for 45 min at room temperature. Nuclei were counterstained by 4′-6-diamidino-2-phenylindole. As a negative control, staining was performed with omission of the primary antibody.

Urate Uptake by VSMC

VSMC (1×10^5) were incubated with 50 μM ^{14}C-urate (American Radiolabeled Chemicals, St. Louis, MO) in Hanks medium (Invitrogen) supplemented with 1 mM L-glutamine (Invitrogen) and 100 μM sodium pyruvate (Invitrogen) for 0, 5, 15, 30, and 60 min at 37°C in a 5% CO_2 incubator. To stop the reaction, we removed the incubation medium and washed the cells three times with ice-cold Hanks medium. The cells were lysed with 0.1 N sodium hydroxide (Sigma) for 20 min, collected into 4-ml scintillation fluid (Fisher Scientific, Pittsburgh, PA) and measured in a β counter (Beckman Coulter Inc., Fullerton, CA). For determination of the specificity of urate uptake, the OAT inhibitor probenecid (1 mM; Sigma) was added to the reaction for the same time course, and samples were collected and measured as described above. All uptake experiments were performed on three separate occasions, and an average value was taken. Data were assessed using a one-way ANOVA with Bonferroni analysis.

Results

First, we examined the mRNA expression of OAT1, OAT2, OAT3, OAT4, and URAT1 in nonstimulated or uric acid–stimulated human aortic VSMC (Figure 1). No detectable expression of OAT1 (573 bp), OAT2 (530 bp), OAT3 (902 bp), or OAT4 (434 bp) mRNA was demonstrated in nonstimulated or uric acid–stimulated VSMC. Nevertheless, expression of OAT1 and OAT3 was present in human kidney, whereas OAT2 and OAT4 were expressed in human liver and placenta, respectively, consistent with their known sites of expression (15–19) (Figure 1).

A band consistent with URAT1 mRNA was observed in both nonstimulated and uric acid–stimulated human VSMC and also in human kidney (365 bp; Figure 1). Forward and reverse

Table 1. Primer sequences for the human organic anion transporters

Gene	Sequence	Corresponding Nucleotides	Annealing Temperature	Number of Cycles	Amplicon Size
hOAT1	Forward: CCA CCT CTT CCT CTG CCT CTC CAT	1266 to 1289	60°C	25	573 bp
	Reverse: GTC TGT TTC CCT TTC CTG CTC TCC	1838 to 1815			
hOAT2	Forward: CTA TCC CCA GGC TCT CCC CAA CAC	252 to 275	62°C	25	530 bp
	Reverse: GAA GCC ATC GCC AGT CCC GTA TCA	781 to 758			
hOAT3	Forward: GCT CTT CTT CCT ATC ATC CTG GTG	740 to 761	60°C	20	902 bp
	Reverse: CTG GCT CCT GCT TTG GCT TCT TTG	1642 to 1619			
hOAT4	Forward: TGC CCT CTT GCT CAG TTT CCT T	1550 to 1571	60°C	30	434 bp
	Reverse: CCT GGG CTG CTG TTG ATT TCT G	1983 to 1962			
hURAT1	Forward: TTG ATT GGC AGG AGG TGA CC	2355 to 2374	60°C	35	365 bp
	Reverse: GGT TAA GTG GAG TCG GTC AG	2719 to 2700			

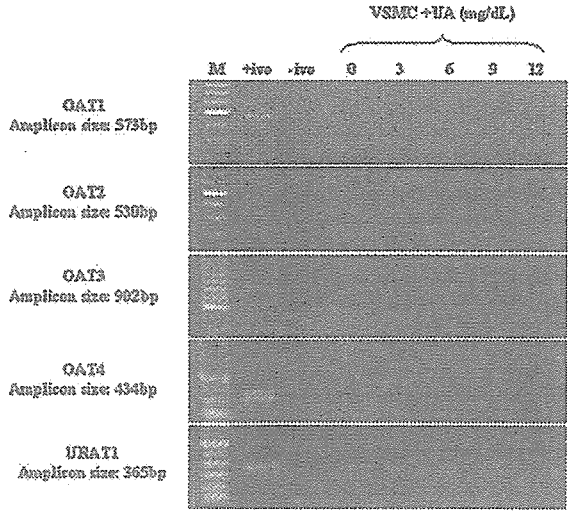

Figure 1. Reverse transcription–PCR (RT-PCR) analysis of URAT1 in nonstimulated and uric acid–stimulated human aortic vascular smooth muscle cells (VSMC). M, 100-bp DNA ladder; +ive, positive control; −ive, without cDNA; 0, VSMC cDNA; 3, VSMC cDNA + 3 mg/dl UA; 6, VSMC cDNA + 6 mg/dl UA; 9, VSMC cDNA + 9 mg/dl UA; 12, VSMC cDNA + 12 mg/dl UA. The organic anion transporter (OAT) URAT1 was expressed in the nonstimulated and uric acid–stimulated (6 h) human aortic VSMC, as assessed by RT-PCR. The results shown are representative of at least three independent experiments. The specificity of the URAT1 observations was also confirmed by both forward and reverse sequencing.

sequencing showed that the PCR products had >99.0% homology with the expected human URAT1 gene sequence (data not shown).

URAT1 protein also was detected in the human VSMC by Western blotting (Figure 2A, top). A band of 40 kD was detected in the nonstimulated and uric acid–stimulated cells. Equality of loading was confirmed by comparative glyceraldehyde-3-phosphate dehydrogenase expression (Figure 2A, bottom).

URAT1 is expressed on the apical membrane of epithelial cells of the human proximal tubule (19). We therefore examined whether URAT1 was expressed on the membrane of human VSMC by Western blot analysis and immunocytochemistry. As can be seen from the representative blot (Figure 2B), URAT1 is expressed on the cell membrane of VSMC. Two bands were detected, one at 40 kD and a second at approximately 50 kD. This observation was confirmed by immunolocalization of URAT1 on human VSMC (Figure 3).

Next, we examined uric acid transport in human VSMC. As shown in Figure 4, uptake of radiolabeled urate increased in VSMC over time, with the highest level being achieved after 60 min. It has been shown that several OAT inhibitors, such as probenecid (19), inhibit the transport of uric acid *via* URAT1. Consistent with this observation, probenecid blocked urate uptake (Figure 4) at all time points, significantly at both 30 and 60 min.

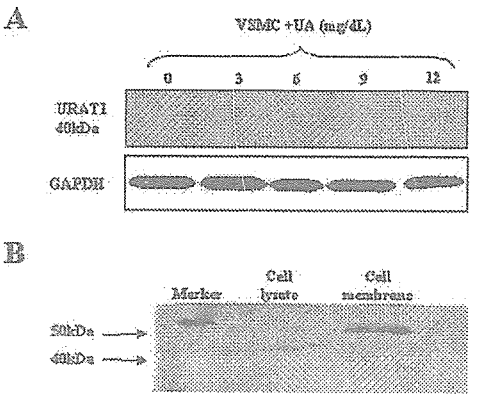

Figure 2. Western blot analysis of URAT1 in human VSMC. (A) Total protein in nonstimulated and uric acid–stimulated VSMC. 0, VSMC cDNA; 3, VSMC cDNA + 3 mg/dl UA; 6, VSMC cDNA + 6 mg/dl UA; 9, VSMC cDNA + 9 mg/dl UA; 12, VSMC cDNA + 12 mg/dl UA. The OAT URAT1 (40 kD) was expressed at similar levels in the nonstimulated and uric acid–stimulated (24 h) human aortic VSMC. Equality of loading was confirmed by comparative glyceraldehyde-3-phosphate dehydrogenase expression. (B) Membrane preparations of human VSMC. The OAT URAT1 was expressed on the membrane of the human aortic VSMC. In both panels, the results shown are representative of at least three independent experiments.

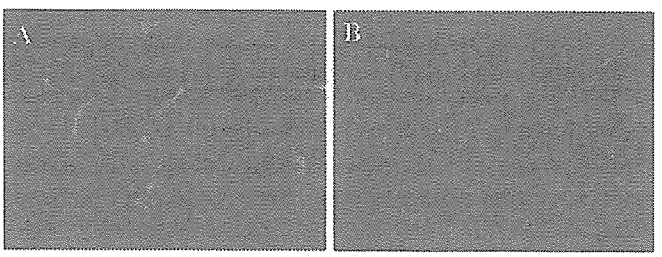

Figure 3. Immunolocalization of URAT1 on human VSMC. Human VSMC were stained overnight with anti-human URAT1 N-terminus affinity-purified antibody followed by donkey anti-rabbit antibody conjugated to Texas Red. (A) URAT1 expression was localized to the cell membrane. (B) Negative control consisted of omission of the primary antibody. For visualization of cell nuclei, cells were stained with 4′-6-diamidino-2-phenylindole.

Discussion

We examined the expression of various OAT in human VSMC. mRNA expression of OAT1, OAT2, OAT3, and OAT4 was not detected in nonstimulated or uric acid–stimulated human aortic VSMC. In contrast, URAT1 mRNA and protein were expressed by both nonstimulated and uric acid–stimulated human VSMC. Consistent with URAT1 being a transporter, we demonstrated the presence of URAT1 on the membrane of these cells. We further showed the presence of a functional OAT in human aortic VSMC, because the cells actively took up urate over a 60-min time course and the uptake was reduced by probenecid. These studies are consistent with previous studies in *Xenopus* oocytes that express URAT1 (19), in which uptake of urate also was significantly inhibited by probenecid.

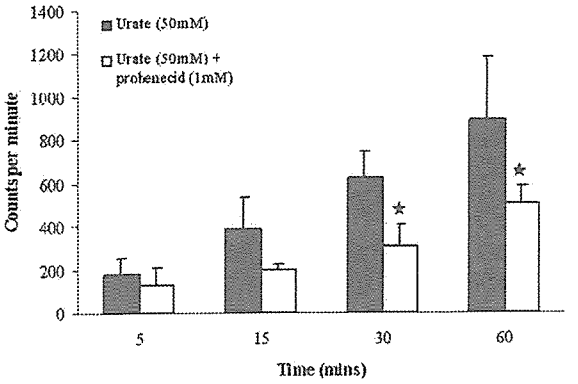

Figure 4. Urate uptake by human VSMC. The function of the URAT1 transporter was assessed by incubating the cells (1×10^5) with ^{14}C-urate over a 60 min time course. At timed intervals, the cells were lysed and the level of urate uptake was measured. Probenecid (1 mM), an inhibitor of OAT, was used to determine specificity of uptake by URAT1 ($P < 0.05$ for 30 and 60 min with probenecid). The experiments were performed on three separate occasions, and the data are displayed as mean counts per minute (± SD).

URAT1 is a recently cloned member of the OAT superfamily and consists of 555 amino acid residues with 12 predicted putative transmembrane domains with both intracellular amino and carboxyl termini (19). Previous studies have demonstrated that URAT1 is expressed prominently on the apical membrane of the proximal tubules but not that of distal tubules in the renal cortex (19). URAT1 transports urate across the apical membrane of proximal tubular cells, with various organic anions being transported in exchange into the tubular lumen to maintain electrical balance (19). Urate then moves across the basolateral membrane into the capillaries *via* another OAT, most likely OAT1 and OAT3 (24). Here we demonstrate the first evidence of a more generalized expression of URAT1 in human VSMC. This novel finding may provide insights into the mechanisms by which uric acid may influence vascular responses in normal and disease states.

The clinical importance of URAT1 is demonstrated by recent studies showing that mutations in the human gene cause idiopathic renal hypouricemia (25,26). This rare disorder occurs with a prevalence of 0.12% in most populations, with a higher frequency in Japanese (27,28) and Iraqi-Jews (24). The disorder is characterized by exercise-induced acute renal failure, triggered by the increased production of urate and reactive oxygen species that occurs in muscle during exercise (25,26). The lack of a functional URAT1 transporter results in lower levels of blood urate and accumulation of urate crystals in kidney tubules, leading to necrosis. Currently, there are no published studies relating hyperuricemia to mutations in URAT1.

Uricosuric agents such as probenecid and benziodarone are commonly used to treat hyperuricemia in patients with gout. It largely has been assumed that these agents are acting solely to inhibit urate reabsorption in the proximal tubule. The observation that URAT1 also is expressed on human VSMC suggests that drugs such as probenecid also may have direct effects on vascular cells. Further studies are planned to determine the role of VSMC expression of URAT1 in normal individuals and patients with cardiovascular disease.

There are several caveats that need to be considered when interpreting the results of this study. First, although we performed forward and reverse sequencing on the PCR products that were obtained from nonstimulated and uric acid–stimulated cells, it would have been optimal to clone and sequence the entire cDNA of URAT1. Second, it would be interesting to explore whether uric acid stimulation alters the expression of URAT1. Although our data suggest that uric acid does not change URAT1 expression, the methods used are nonquantitative. Therefore, further studies need to be performed using techniques such as real-time PCR or Northern analysis. Finally, the data obtained with radiolabeled urate and the addition of probenecid are suggestive of a functional uric acid transporter in human VSMC. However, it should be noted that the concentration of probenecid used may be too low to block urate uptake completely. In addition, other inhibitors such as benzbromarone may be more specific for URAT1 (29). Indeed, to prove definitively that URAT1 is a functional transporter, experiments with antisense constructs or small interfering RNA need to be performed.

Acknowledgments

Support for the research is provided by National Institutes of Health grants DK-52121, HL-68607, and KD-64233. D.A.L is supported by a Bogue Research Fellowship, University College, London.

References

1. Johnson RJ, Kang DH, Feig D, Kivlighn S, Kanellis J, Watanabe S, Tuttle KR, Rodriguez-Iturbe B, Herrara-Acosta J, Mazzali M: Is there a pathogenetic role for uric acid on hypertension and cardiovascular and renal disease? *Hypertension* 41: 1183–1190, 2003
2. Wu XW, Muzny DM, Lee CC, Caskey CT: Two independent mutational events in the loss of urate oxidase during hominoid evolution. *J Mol Evol* 34: 78–84, 1992
3. Cannon PJ, Statson WB, Demartini FE, Sommers SC, Laragh JH: Hyperuricemia in primary and renal hypertension. *N Engl J Med* 275: 457–464, 1966
4. Selby JV, Friedman GD, Quesenberry CP Jr: Precursors of essential hypertension: Pulmonary function, heart rate, uric acid, serum cholesterol and other serum chemistries. *Am J Epidemiol* 131: 1017–1027, 1990
5. Messerli FH, Frohlich ED, Dreslinski GR, Suarez DH, Aristimuno GG: Serum uric acid in essential hypertension: An indicator of renal vascular involvement. *Arch Intern Med* 93: 817–821, 1980
6. Feig DI, Johnson RJ: Hyperuricemia in childhood primary hypertension. *Hypertension* 42: 247–252, 2003
7. Mazzali M, Hughes J, Kim YG, Jefferson JA, Kang DH, Gordon KL, Lan HY, Kivlighn S, Johnson RJ: Elevated uric acid increases blood pressure in the rat by a novel crystal-independent mechanism. *Hypertension* 38: 1101–1106, 2001
8. Mazzali M, Kanellis J, Han L, Feng L, Xia YY, Chen Q, Kang DH, Gordon KL, Nakagawa T, Lan HY, Johnson RJ: Hyperuricemia induces a primary arteriopathy in rats by a

blood pressure-independent mechanism. *Am J Physiol Renal Physiol* 282: F991–F997, 2002
9. Sanchez-Lozada LG, Tapia E, Avila-Casado C, Soto V, Franco M, Santamaria J, Nakagawa T, Rodriguez-Iturbe B, Johnson RJ, Herrara-Acosta J: Mild hyperuricemia induces glomerular hypertension in normal rats. *Am J Physiol Renal Physiol* 283: F1105–F1110, 2002
10. Nakagawa T, Mazzali M, Kang DH, Kanellis J, Watanabe S, Sanchez-Lozada LG, Rodriguez-Itrube B, Herrera-Acosta J, Johnson RJ: Hyperuricemia causes glomerular hypertrophy in the rat. *Am J Nephrol* 23: 2–7, 2003
11. Khosla UM, Zharikov S, Finch JL, Nakagawa T, Roncal C, Mu W, Krotova K, Block ER, Prabhakar S, Johnson RJ: Hyperuricemia induces endothelial dysfunction. *Kidney Int* 67: 1739–1742, 2005
12. Rao GN, Corson MA, Berk BC: Uric acid stimulates vascular smooth muscle cell proliferation by increasing platelet-derived growth factor A-chain expression. *J Biol Chem* 266: 8604–8608, 1991
13. Kanellis J, Watanabe S, Li JH, Kang DH: Li P, Nakagawa T, Wamsley A, Sheikh-Hamad D, Lan HY, Feng L, Johnson RJ: Uric acid stimulates monocyte chemoattractant protein-1 production in vascular smooth muscle cells via mitogen-activated protein kinase and cyclooxygenase-2. *Hypertension* 41: 1287–1293, 2003
14. Kang DH, Park SK, Lee IK, Johnson RJ: Uric acid-induced C-reactive protein expression: Implication on cell proliferation and nitric oxide production of human vascular cells. *J Am Soc Nephrol* 16: 3553–3562, 2005
15. Sekine T, Watanabe N, Hosoyamada M, Kanai Y, Endou H: Expression cloning and characterization of a novel multispecific organic anion transporter. *J Biol Chem* 272: 18526–18529, 1997
16. Sekine T, Cha SH, Tsuda M, Apiwattanakul N, Nakajima N, Kanai Y, Endou H: Identification of multispecific organic transporter 2 expressed predominantly in the liver. *FEBS Lett* 429: 179–182, 1998
17. Kusuhara H, Sekine T, Utsunomiya-Tate N, Tsuda M, Kojima R, Cha SH, Sugiyama Y, Kanai Y, Endou H: Molecular cloning and characterization of a new multispecific organic anion transporter from rat brain. *J Biol Chem* 274: 13675–13680, 1999
18. Cha SH, Sekine T, Kusuhara H, Yu E, Kim JY, Kim DK, Sugiyama Y, Kanai Y, Endou H: Molecular cloning and characterization of multispecific organic anion transporter 4 expressed in the placenta. *J Biol Chem* 275: 4507–4512, 2000
19. Enomoto A, Kimura H, Chairoungdua A, Shigeta Y, Jutabha P, Cha SH, Hosayamada M, Takeda M, Sekine T, Igarashi T, Matsuo H, Kikuchi Y, Oda T, Ichida K, Hosoya T, Shimokata K, Niwa T, Kanai Y, Endou H: Molecular identification of a renal urate anion exchanger that regulates blood urate levels. *Nature* 417: 447–452, 2002
20. Sekine T, Cha SH, Endou H: The multispecific organic anion transporter (OAT) family. *Pflugers Arch* 440: 337–350, 2000
21. Kang DH, Han L, Ouyang X, Kahn AM, Kanellis J, Li P, Feng L, Nakagawa T, Watanabe S, Hosoyamada M, Endou H, Lipkowitz M, Abramson R, Mu W, Johnson RJ: Uric acid causes vascular smooth muscle cell proliferation by entering cells via a functional urate transporter. *Am J Nephrol* 25: 425–433, 2005
22. Bornfeldt KE, Raines EW, Nakano T, Graves LM, Krebs EG, Ross R: Insulin-like growth factor-1 and platelet-derived growth factor BB induce directed migration of human arterial smooth muscle cells via signalling pathways that are distinct from those of proliferation. *J Clin Invest* 93: 1266–1274, 1994
23. Long DA, Woolf AS, Suda T, Yuan HT: Increased renal angiopoietin-1 expression in folic acid-induced nephrotoxicity in mice. *J Am Soc Nephrol* 12: 2721–2731, 2001
24. Hediger MA, Johnson RJ, Miyazaki H, Endou H: Molecular physiology of urate transport. *Physiology* 20: 125–133, 2005
25. Kikuchi Y, Koga H, Yasutomo Y, Kawabata Y, Shimizu E, Naruse M, Kiyama S, Nonoguchi H, Tomita K, Sasatomi Y, Takebayashi S: Patients with renal hypouricemia with exercise-induced acute renal failure and chronic renal dysfunction. *Clin Nephrol* 53: 467–472, 2000
26. Igarashi T, Sekine T, Sugimura H, Hayakawa H, Arayama T: Acute renal failure after exercise in a child with renal hypouricemia. *Pediatr Nephrol* 7: 272–293, 1993
27. Ichida K, Hosoyamada M, Hisatome I, Enomoto A, Hikita M, Endou H, Hosoya T: Clinical and molecular analysis of patients with renal hypouricemia in Japan-influence of URAT1 gene on urinary urate excretion. *J Am Soc Nephrol* 15: 164–173, 2004
28. Kwai N, Mino Y, Hosoyamada M, Tago N, Kokubo Y, Endou H: A high prevalence of renal hypouricemia caused by inactive SLC22A112 in Japanese. *Kidney Int* 66: 935–944, 2004
29. Iwanaga T, Kobayashi D, Hirayama M, Maeda T, Tamai I: Involvement of uric acid transporter in increased renal clearance of the xanthine oxidase inhibitor oxypurinol induced by a uricosuric agent, benzbromarone. *Drug Metab Dispos* 33: 1791–1795, 2005

Please see the related editorial, "Uric Acid: An Old Dog with New Tricks," on pages 1767–1768.

A novel missense mutation of *SLC7A9* frequent in Japanese cystinuria cases affecting the C-terminus of the transporter

Y Shigeta[1,2], Y Kanai[1], A Chairoungdua[1], N Ahmed[1,2], S Sakamoto[1,2], H Matsuo[1,3], DK Kim[1,4], M Fujimura[1,2], N Anzai[1], K Mizoguchi[2], T Ueda[2], K Akakura[2], T Ichikawa[2], H Ito[2] and H Endou[1]

[1]Department of Pharmacology and Toxicology, Kyorin University School of Medicine, Shinkawa, Mitaka, Tokyo, Japan; [2]Department of Urology, Chiba University Graduate School of Medicine, Inohana, Chuo-Ku, Chiba, Japan; [3]First Department of Physiology, National Defense Medical College, , Tokorozawa, Saitama, Japan and [4]Department of Oral Physiology, Chosun University College of Dentistry, Gwangju, Korea

Cystinuria is caused by the inherited defect of apical membrane transport systems for cystine and dibasic amino acids in renal proximal tubules. Mutations in either *SLC7A9* or *SLC3A1* gene result in cystinuria. The mutations of *SLC7A9* gene have been identified mainly from Italian, Libyan Jewish, North American, and Spanish patients. In the present study, we have analyzed cystinuria cases from oriental population (mostly Japanese). Mutation analyses of *SLC7A9* and *SLC3A1* genes were performed on 41 cystinuria patients. The uptake of ^{14}C-labeled cystine in COS-7 cells was measured to determine the functional properties of mutants. The protein expression and localization were examined by Western blot and confocal laser-scanning microscopy. Among 41 patients analyzed, 35 were found to possess mutations in *SLC7A9*. The most frequent one was a novel missense mutation P482L that affects a residue near the C-terminus end of the protein and causes severe loss of function. In MDCK II and HEK293 cells, we found that P482L protein was expressed and sorted to the plasma membrane as well as wild type. The alteration of Pro^{482} with amino acids with bulky side chains reduced the transport function of $b^{0,+}$AT/BAT1. Interestingly, the mutations of *SLC7A9* for Japanese cystinuria patients are different from those reported for European and American population. The results of the present study contribute toward understanding the distribution and frequency of cystinuria-related mutations of *SLC7A9*.

Kidney International (2006) **69,** 1198–1206. doi:10.1038/sj.ki.5000241; published online 1 March 2006

KEYWORDS: cystinuria; epithelial transport; membrane transporter; proximal tubule

Correspondence: *Y Kanai, Department of Pharmacology and Toxicology, Kyorin University School of Medicine, 6-20-2 Shinkawa, Mitaka, Tokyo 181-8611, Japan. E-mail: ykanai@kyorin-u.ac.jp*

Received 29 July 2005; revised 8 October 2005; accepted 28 October 2005; published online 1 March 2006

Cystinuria (MIM 220100) is an inherited disorder owing to the defective transport of cystine and dibasic amino acids across the epithelial cells of renal proximal tubule and small intestine.[1] The incidence of cystine crystalluria reported in Western countries and in Japan varied from 15 000:1 to 50 000:1.[2,3] The patients suffer from recurrent nephrolithiasis leading to severe renal dysfunctions for which repeated therapies are imperative.[4] Classical cystinuria has been classified into three types (I, II, and III) based on the excretion of cystine and dibasic amino acids in obligate heterozygotes.[5] Type I heterozygotes show a normal amino-acid urinary pattern, whereas type II and III heterozygotes exhibit high or moderate levels of hyperexcretion of cystine and dibasic amino acids.[5] The discovery of a single-membrane-spanning type II membrane glycoprotein rBAT encoded by *SLC3A1*[6–10] and 12-membrane-spanning protein $b^{0,+}$AT/BAT1 encoded by *SLC7A9*[11–13] has brought a breakthrough in the understanding of the molecular basis of cystinuria and cystine transport in the renal proximal tubules.

The analyses of cystinuria patients have revealed distinct cystinuria-related mutations in *SLC3A1* and *SLC7A9* genes.[14,15] It was originally supposed that mutations of *SLC3A1* and *SLC7A9* genes are responsible for type I and non-type I (type II and III) cystinuria, respectively. However, recent developments in the genetics and physiology of cystinuria have not supported such a traditional classification.[16–18] Although *SLC3A1* is associated with the type I urinary phenotype, *SLC7A9* mutations were found in all three subtypes.[16,17] Therefore, a new cystinuria classification based on molecular analysis and not on urinary amino-acid excretion patterns has been proposed: type A, due to two mutations of *SLC3A1*; type B, due to two mutations of *SLC7A9*; and type AB, with one mutation on each of the above-mentioned genes.[17] For *SLC7A9* gene, International Cystinuria Consortium and Rozen and colleagues identified cystinuria-related mutations mainly from Italian, Libyan Jewish, North American, and Spanish patients

and established the genotype–phenotype relation for *SLC7A9*.[12,16–18] In the present study, we have analyzed cystinuria cases from oriental population (mostly Japanese) and found that the mutations of *SLC7A9* for Japanese cystinuria patients are quite different from those reported for European, North American, and Libyan Jewish. We report here that the most frequent one is a novel missense mutation affecting the C-terminus of the transporter protein (Tables 1 and 2).

RESULTS

Mutations of *SLC7A9* and *SLC3A1* found in cystinuria patients

We studied 41 cystinuria patients from 39 cystinuria families potentially representing 78 independent cystinuria-related alleles. They were subjected to the mutation analysis of *SLC7A9* gene by direct sequencing. The mutations of *SLC7A9* gene found in the cystinuria patients are listed in Table 3. They include one frameshift (1105delA) and one nonsense mutation (W69stop) that produce early stop codons, and seven changes affecting single amino-acid residues (V142A, G195R, L223M, N227D, R333W, R333Q, and P482L). Among them, V142A, L223M, N227D, R333Q, 1105delA, and P482L were novel mutations found for the first time in the present investigation, whereas three mutations (W69stop, G195R, and R333W) were reported previously for the European, North American, and Libyan Jewish population.[12,16,18] The amino-acid alterations except V142A and L223M were not found in 50 normal subjects. V142A and L223M were, in contrast, found in normal subjects without cystinuria phenotype. V142A and L223M were found in 23 and 19 alleles out of 50 normal subjects (100 independent alleles), respectively, suggesting that these amino-acid alterations represent polymorphic variations of *SLC7A9*.

The location of the *SLC7A9* mutations is shown at the corresponding amino-acid residues in the 12-transmembrane (TM)-domain model of $b^{0,+}$AT/BAT1 protein in Figure 1. Five cystinuria-specific missense mutations were localized within the putative TM domains 5 and 6 (G195R and N227D), in the putative intracellular loop between TM8 and TM9 (R333W and R333Q), or in the C-terminus (P482L). The one single nucleotide deletion is localized to the portion corresponding to the putative intracellular loops between TM8 and TM9 (1105delA). Three mutations (G195R, R333W, and R333Q) alter amino-acid residues that are conserved for all the human members of the heterodimeric amino-acid transporter family (Figure 1).

Among 41 cystinuria patients examined in the present study, we found mutations of *SLC3A1* in five cases. Two cases without any alterations in *SLC7A9* gene possessed mutations for *SLC3A1*: one as a homozygote for the deletion of T at nucleotide 1820; the other as a compound heterozygote for V183A (T548C)/C673R (T2017C); nucleotide numbers refer to GenBank accession no. NM_000341 for rBAT cDNA.[19] Among four cases with only polymorphic changes (V142A and/or L223M) in *SLC7A9*, two cases possessed mutations for *SLC3A1*: one as a homozygote for the insertion of TA at nucleotide 1898; the other as a compound heterozygote for V183A (T548C)/L346P (T1037C). The other two cases with only polymorphic changes in *SLC7A9* did not possess *SLC3A1* mutations. *SLC3A1* mutations were not found in the cases with cystinuria-specific mutations of *SLC7A9* except one P482L homozygote that also possesses I445T (T1334C) mutation in *SLC3A1*.

Functional analysis of *SLC7A9* mutations

All the *SLC7A9* mutations found in the present study were examined for amino-acid transport activity. As shown in Figure 2, the cystinuria-specific mutations such as W69stop, G195R, N227D, R333Q, R333W, 1105delA, and P482L exhibited remarkable decrease in cystine transport activity compared with wild-type $b^{0,+}$AT/BAT1. In contrast, V142A and L223M, which were also found in normal subjects, did not affect or only slightly decreased the cystine transport activity compared with wild-type $b^{0,+}$AT/BAT1 (Figure 2). We also constructed V142A/L223M double mutant, which contains both V142A and L223M alterations because they are possibly located in the same allele. As shown in Figure 2, even the double mutation for V142A and L223M did not severely affect the functional activity.

Table 1 | Primers used for amplification of *SLC7A9* exons and their direct sequencing

	Sense primer	Antisense primer	Size of amplified fragment
Exon 2	5′-GAGCTTGCACTTGCGTCTTG-3′	5′-AATCAAAGAGTACATCTTCTGCCG-3′	299[a]
Exon 3	5′-TGGCCTTCTGGGCTGGGTC-3′	5′-AAGAGGGATACTGGCAGGGT-3′	307
Exon 4[b]	5′-AGCCTCCGGTGGGAGGAAG-3′	5′-GAGTCCCCAGACACCCTCTG-3′	388
Exon 5[b]	5′-AAAGGAGACTCTCTCCAGGG-3′	5′-ATGCTTCCTTGGAGATGGGCT-3′	292
Exon 6	5′-CCATCTTTCCCGTGGAGATACA-3′	5′-CAAACCCCAGAAAGGAGAACTC-3′	279
Exon 7	5′-CCACTAGCAGGGCCATTCAC-3′	5′-CGGGAAGGGCATCATGGAATAC-3′	316
Exon 8[b]	5′-CTGAACGTGGGTCTCCGTG-3′	5′-ACCTCCAGTGCTGACACCTG-3′	235
Exon 9	5′-CTCTTGGAGGCCGAGAAAGAC-3′	5′-GGGTGTTATTGCTTTCGCCGC-3′	214
Exon 10	5′-TGGTCTGCACTCTGGTCAGC-3′	5′-GGCATCTGGGTCATTTGGAAG-3	236
Exon 11	5′-CTTCTTCGGTCTTCTGTGAC-3′	5′-CTAGAAGGCATGCCCCTAGC-3′	314
Exon 12	5′-AGGGGGTACATGGAGTTCATAC-3′	5′-GTGACAGAGGTCTTGGAGTC-3′	366
Exon 13	5′-CAGGGTCTAGGTGACGCATC-3′	5′-TCAGCTGACTTGGCTACAAGAG-3′	218

[a]The size of the fragments amplified by PCR using sense and antisense primers described is indicated (bp).
[b]The primers for exons 4, 5, and 8 are identical to those for reference International Cystinuria Consortium.[12]

Table 2 | The mutagenic oligonucleotide primers[a]

SLC7A9 mutagenesis primers	
W69stop	5′-CCTGCCTCATCATAT(A)[b]GGCGGCTTGCGGGG-3′
G195R	5′-CATCATCATCATCAGC(A)GGCTGGTGCTCCTGGC-3′
V142A	5′-GTGCGCCCTTCTATG(C)GGGCTGCAAGCCTC-3′
L223M	5′-GGGAGCCATCAGC(A)TGGCGTTTTACAATGG-3′
N227D	5′-CCTGGCGTTTTAC(G)ATGGACTCTGGGCC-3′
R333Q	5′-CATTTACGTGGCGGGC(A)GGGAGGGTCACATG-3′
R333W	5′-CATTTACGTGGCGGGC(T)GGGAGGGTCACATG-3′
1105delA	5′-GGGTCACATGCTCAAA*GTGCTTTCTTAC-3′
P482L	5-GGAAGTGGTCCCAC(T)GGAGGAAGACCC-3
Alanine mutagenesis primers	
M477A	5′-GCACCTTCAGATGCTA(GC)GGAAGTGGTCCCAC-3′
E478A	5′-CTTCAGATGCTAATGG(CC)GTGGTCCCACCGGA-3′
V479A	5′-CAGATGCTAATGGAAG(CG)GTCCCACCGGAGGA-3′
V480A	5′-ATGCTAATGGAAGTGG(C)CCCACCGGAGGAAGA-3′
P481A	5′-GCTAATGGAAGTGGTC(G)CACCGGAGGAAGACC-3′
E483A	5′-GAAGTGGTCCCACCGG(CT)GAAGACCCTGAGTA-3′
E484A	5′-GTGGTCCCACCGGAGG(C)AGACCCTGAGTAACA-3′
D485A	5′-GTCCCACCGGAGGAAG(C)CCCTGAGTAACAAGC-3′
P486A	5′-CCCACCGGAGGAAGAC(G)CTGAGTAACAAGCTC-3′
E487A	5′-CCGGAGGAAGACCCTG(C)GTAACAAGCTCCGTC-3′,
Leucine mutagenesis primers	
M477L	5′-CTTCAGATGCTA(C)TGGAAGTGGTCCC-3′
E478L	5″-CGAATGCTAATG(CT)AGTGGTCCCACC-3′
V479L	5-GATGCTAATGGAA(C)TGGTCCCACCGGAG-3′
V480L	5′-CTAATGGAAGTG(C)TCCCACCGGAGGA-3′
P481L	5′-ATGGAAGTGGTC(C)TACCGGAGGAAGAC-3′
E483L	5′-GTGGTCCCACCG(CT)GGAAGACCCTGAG-3′
E484L	5′-GGTCCCACCGGAG(CT)AGACCCTGAGTAAC-3′
D485L	5′-CCACCGGAGGAA(CT)CCCTGAGTAACA-3′
P486L	5′-CCAGTAGGAAGACC(T)TGAGTAACAAGCTC-3′
E487L	5′-GGAGGAAGACCCT(CT)GTAACAAGCTCC-3′
P482X mutation primers	
P482G	5′-GGAAGTGGTGCCA(GG)GGAGGAAGACCCTG-3′
P482A	5′-GGAAGTGGTCCCA(G)CGGAGGAAGACCCTG-3′
P482S	5′-GGAAGTGGTCCCA(T)CGGAGGAAGACCCTG-3′
P482V	5′-GGAAGTGGTCCCA(GT)GGAGGAAGACCCTG-3′
P482I	5′-GGAAGTGGTCCCA(ATT)GAGGAAGACCCTG-3′
P482M	5′-GGAAGTGGTCCCA(AT)GGAGGAAGACCCTG-S[1]
P482F	5′-GGAAGTGGTCCCA(TTC)GAGGAAGACCCTG-3′
P482W	5′-GGAAGTGGTCCCA(TG)GGAGGAAGACCCTG-3′

[a]Sense strand primers are shown.
[b]Mutated nucleotides are shown in parentheses.
*One nucleotide has been deleted.

P482L mutation

Among 41 cystinuria patients examined, cystinuria-specific mutations of *SLC7A9* excluding apparently polymorphic changes (V142A and L223M) were found in 35 cases (Table 3). It is noted that 25 cases were P482L homozygotes and six cases were heterozygotes involving P482L mutations. Urinary excretion levels of cystine and basic amino acids in the P482L homozygotes, compound heterozygotes involving P482L mutations, and P482L obligate heterozygotes who exhibited no cystinuria symptoms are provided in Table 4. P482L homozygotes and compound heterozygotes exhibited a high level of urinary excretion of cystine, lysine, arginine, and ornithine, whereas P482L obligate heterozygotes exhibited a significantly lower level of excretion of these amino acids, which is still higher than the normal levels (Table 4).

We further examined two family pedigrees with P482L mutation (Figure 3). In Family 1, the proband 1-6 with a clinical history of nephrolithiasis was homozygous for P482L and showed a high level of excretion of cystine and dibasic amino acids (Table 5). The heterozygotes 1-2 and 1-3 showed a lower level of amino acid excretion (Table 5). The urinary amino acid excretion of 1-1 and 1-5 without P482L mutation was within the normal range. In Family 2, 2-3 and 2-5 were homozygous for P482L, which showed a high level of urinary amino acid excretion. Although 2-2 exhibited a relatively high urinary excretion level for a heterozygote, she did not have an episode of delivery or removal of cystine stones.

Protein characterization of $b^{0,+}$AT/BAT1 mutants

We performed Western blot analyses using an antibody raised against the C-terminus portion of human $b^{0,+}$AT/BAT1 on the crude membrane fractions prepared from COS-7 cells coexpressing wild-type or mutant $b^{0,+}$AT/BAT1 with rBAT. The antibody recognized a 41 kDa protein for wild-type $b^{0,+}$AT/BAT1 in the Western blot (Figure 4a). The band disappeared in the presence of antigen peptides in the absorption experiment, confirming the specificity of immunoreactions (data not shown). As shown in Figure 4a, the bands with the identical size were detected for G195R, N227D, R333W, and R333Q mutants. The anti-C-terminus antibody could not detect W69stop and 1105delA, which lack the C-terminus portions. Furthermore, the antibody could not detect P482L, which has a mutation in the C-terminus region for which the antibody was generated (Figure 4a).

We further performed Western blot analyses using an anti-myc antibody on the membrane fractions prepared from COS-7 cells coexpressing myc-tagged wild-type or mutated $b^{0,+}$AT/BAT1 with rBAT. The anti-myc antibody recognized the bands with identical size as those detected by the anti-$b^{0,+}$AT/BAT1 C-terminus antibody (Figure 4b). The rank order of the relative band intensity of myc fusion proteins for G195R, N227D, R333W, and R333Q mutants determined by the anti-myc antibody was identical to that of G195R, N227D, R333W, and R333Q detected by the anti-C-terminus antibody. The anti-myc antibody did not detect the protein products of W69stop (~7 kDa) and 1105delA (~38 kDa) with a myc epitope on their N-termini. In contrast to the anti-C-terminus antibody, the anti-myc antibody recognized the P482L with a myc epitope on its N-terminus (myc-P482L), indicating that myc-P482L is present almost in the same amount as that for wild-type $b^{0,+}$AT/BAT1 (Figure 4b).

Localization of wild-type and P482L proteins in polarized MDCK II cells

In order to determine the subcellular localization of P482L protein, we performed confocal fluorescence analysis on the MDCK II cells expressing GFP-$b^{0,+}$AT/BAT1 (GFP: green fluorescent protein) alone or both myc-rBAT and GFP-$b^{0,+}$AT/BAT1 or GFP-P482L. For the coexpression experiments, the cells positive for both GFP fluorescence and Alexa Fluor fluorescence (myc-rBAT positive) were used for the

Table 3 | Summary of $b^{0,+}$AT/BAT1 mutations in cystinuria patients

Mutation type	Status	Nucleotide change	Exon	Protein domain	Urinary cystine (nmol/mg Cr)	Number of patients
P482L	Homozygote	C1533T	13	C-terminus	2065.8±305.3[a]	25
P482L	Heterozygote	C1533T	13	C-terminus	ND	3
P482L	Compound heterozygote	G671A	5	TM5		
G195R		C1533T	13	C-terminus	2103.5	1
P482L	Compound heterozygote	C1085T	10	IL4		
R333W		C1533T	13	C-terminus	2628.4	1
P482L	Compound heterozygote	G1086A	10	IL4		
R333Q		C1533T	13	C-terminus	ND	1
R333Q	Homozygote	G1086A	10	IL4	ND	1
N227D	Heterozygote	A767G	6	TM6	ND	1
1105delA[b]	Homozygote	1105delA	10	IL4	2118.0	1
W69stop	Compound heterozygote	G294A		TM2		
1105delA[b]		1105delA	3	IL4	ND	1
V142A	Heterozygote[c]	T513C	4	EL2		
L223M		C755A	6	TM6	ND	4
Total						39

[a]Mean±s.e.m. (n=7).
[b]1105delA results in the frameshift after Val^{340}.
[c]It is not known whether V142A and L223M mutations of these patients are in the same alleles or not.
ND, urinary cystine level was not determined for these cases. Instead, urinary cystine excretion was confirmed by cyanide-nitroprusside test. Cystine stones were also confirmed by infrared spectrophotometry.

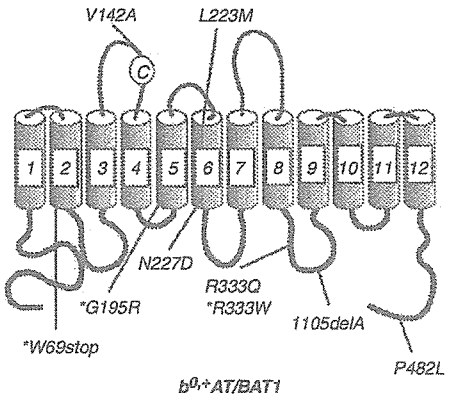

Figure 1 | Schematic representation of the mutations found in *SLC7A9* gene of patients with cystinuria. Nine mutations in *SLC7A9* gene found in 41 cystinuria patients are depicted at the corresponding amino acid residues in the 12-TM-domain model of $b^{0,+}$AT/BAT1 protein.[26] Seven mutations (W69stop, G195R, N227D, R333W, R333Q, 1105delA, and P482L) were cystinuria-specific, whereas two (V142A and L223M) were also found in the normal subjects (see text). W69stop, G195R, and N227D are located within the putative TM domains. R333Q, R333W, 1105delA, and P482L are located in the proposed intracellular loops or in the C-terminus intracellular domain. The mutations reported previously[12,16,18] were labeled with *.

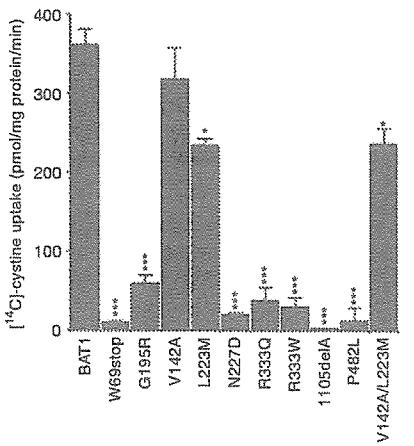

Figure 2 | Effects of *SLC7A9* mutations on the cystine transport activity. Wild-type $b^{0,+}$AT/BAT1 and indicated mutants were transiently expressed in COS-7 cells together with rBAT. The uptake of [^{14}C]L-cystine (100 μM) mediated by the expressed proteins was measured as described in 'Materials and Methods'. All transport values except those for V142A were significantly lower than those for wild-type coexpressed with rBAT. The transport values for L223M and V142A/L223M were higher than those for W69stop, G195R, N227D, R333Q, R333W, 1105delA, or P482L. V142A/L223M is a mutant that contains both V142A and L223M mutations. Asterisks indicate statistical significance (*$P<0.05$; ***$P<0.005$, Student's unpaired t-test).

analyses. As shown in Figure 5a, GFP-$b^{0,+}$AT/BAT1 protein was localized in the cytoplasm when expressed alone in MDCK II cells. Coexpression of GFP-$b^{0,+}$AT/BAT1 with myc-rBAT resulted in the apical localization of GFP-$b^{0,+}$AT/BAT1 protein in the MDCK II cells (Figure 5b). Similarly, GFP-P482L protein was also localized to the apical membrane when coexpressed with myc-rBAT (Figure 5c).

The plasma membrane expression of $b^{0,+}$AT/BAT1 and P482L proteins was further confirmed by surface biotinylation analysis (Figure 5d). HEK293 cells were used in this experiment for their higher efficiency in biotinylation analysis, probably due to the higher expression of the proteins. Consistent with the observation in COS-7 cells, myc-$b^{0,+}$AT/BAT1 but not myc-P482L showed

Table 4 | Urine amino acid levels in P482L homozygotes, compound heterozygotes, and obligate heterozygotes

		n	Cystine	Lysine	Arginine	Ornithine
P482L/P482L	Homozygotes	7	2065.8±305.3[a] (965.9–3056.6)[b]	8270.9±1185.3 (3866.8–11860.7)	3299.3±349.9 (1729.3–4482.8)	2233.0±383 (1032.1–4150.2)
R333W+P482L	Compound heterozygotes	1	2628.4	8855.4	3407.1	1592.7
G195R+P482L	Compound heterozygotes	1	2103.5	12911.5	6396.8	3744.5
P482L/+	Obligate heterozygotes	7	603.0±174.7[a, **] (56.3–1417.8)[b]	2534.7±623.5** (172.7–4781.8)	75.7±13.8** (25.6–118.4)	170.9±62.0** (18.2–354.5)
	Normal range		20–150	50–1300	10–60	5–40 (nmol/mg creatinine)

[a]Mean±s.e.m. (n=7).
[b]Range of amino acid excretion levels.
**$P<0.01$, versus homozygotes and compound heterozygotes (Mann–Whitney U-test).

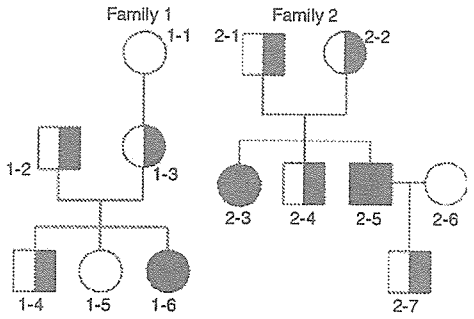

Figure 3 | Pedigrees of Japanese cystinuria families with P482L mutation. Two Japanese families (Families 1 and 2) with P482L mutation examined are shown.

Table 5 | Urinary excretion levels of cystine and dibasic amino acids of two family pedigrees

Individual no.[a]	Cystine	Lysine	Arginine	Ornithine	Sum
1-1	32.8	102.9	193.7	51.9	381.3
1-2	160.3	904.2	22.5	21	1108
1-3	791.1	3164.1	107.9	328.8	4391.9
1-4	385	2912.5	61.6	60.5	3419.6
1-5	64.7	222.8	23.1	20.1	330.7
1-6[b]	2240	7049	3538.3	2026.1	14853.4
2-1	255.6	1062.4	33.6	42.7	1394.3
2-2	1417.8	4012.9	100.3	354.5	5885.5
2-3	2932.6	9726.3	3440.7	2364.4	18464
2-4	ND	ND	ND	ND	ND
2-5[b]	1677.9	6370	2478.8	1692.7	12219.4
2-6	ND	ND	ND	ND	ND
2-7	891.7	4781.8	118.4	352.9	6144.8
Normal range	20–150	50–1300	10–60	5–40	(nmol/mg creatinine)

[a]The individual numbers are corresponded to those of members of the family pedigrees shown in Figure 4.
[b]1-6 and 2-5 are probands.
ND, Not determined.

$[^{14}C]$L-cystine uptake when coexpressed with rBAT in HEK293 cells (data not shown). As shown in Figure 5d, myc-$b^{0,+}$AT/BAT1 and myc-P482L proteins were detected at the plasma membrane when coexpressed with rBAT. The myc-$b^{0,+}$AT/BAT1 and myc-P482L proteins were not detected at plasma membrane when solely expressed (Figure 5d).

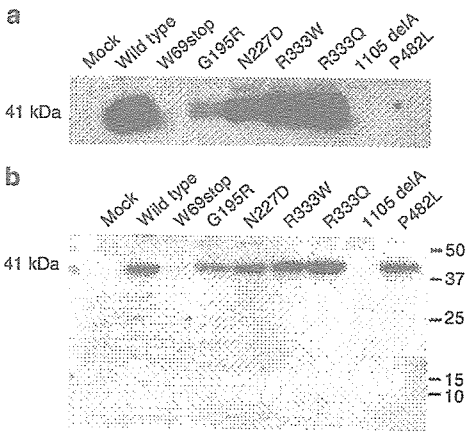

Figure 4 | Western blot analysis of $b^{0,+}$AT/BAT1 and its mutants. (**a**) $b^{0,+}$AT/BAT1 and its mutants were transiently expressed in COS-7 cells with rBAT. The Western blot analysis using an anti-$b^{0,+}$AT/BAT1 C-terminus antibody was performed on the membrane fraction prepared from the COS-7 cells. The anti-$b^{0,+}$AT/BAT1 C-terminus antibody recognized a 41 kDa band for wild-type $b^{0,+}$AT/BAT1 and its mutants except W69stop, 1105delA, and P482L. (**b**) An anti-myc antibody was used to detect $b^{0,+}$AT/BAT1 and its mutants to which a myc epitope was added at their N-termini. The myc-tagged proteins were transiently expressed in COS-7 cells with rBAT. In the Western blot, the anti-myc antibody recognized a 41 kDa band for wild-type $b^{0,+}$AT/BAT1 and its mutants including P482L.

Effect of P482L mutation

In order to understand why P482L, a single amino acid alteration at the C-terminus of the transporter protein, resulted in the loss of transport function, we performed site-directed mutagenesis analyses. For the series of mutants in which residues between Met^{477} and Glu^{487} were systematically changed to alanine, no remarkable decrease was observed in the $[^{14}C]$L-cystine transport activity compared with wild-type $b^{0,+}$AT/BAT1 (Figure 6a). It is notable that the alteration of Pro^{482} to alanine did not affect the $[^{14}C]$L-cystine transport activity in contrast to the severe decrease in the transport activity observed for P482L. We, then, changed individual amino acid residues located between residues 477 and 487 to leucine (Figure 6b). We found that P481L, V479L, M477L, E478L, and V480L, in addition to P482L, exhibited a significant decease in the $[^{14}C]$L-cystine transport activity

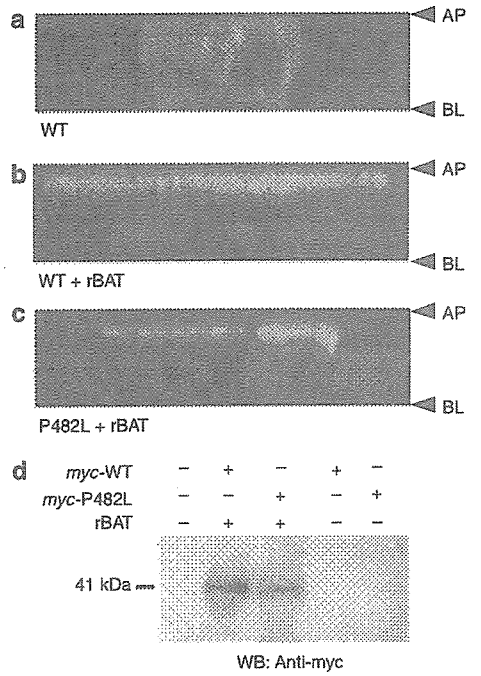

Figure 5 | Localization of P482L protein on the plasma membrane. Shown are the *x–z* images of confocal laser-scanning microscopic analyses on the MDCK II cells expressing (**a**) GFP-$b^{0,+}$AT/BAT1, (**b**) GFP-$b^{0,+}$AT/BAT1 with rBAT, and (**c**) GFP-P482L with rBAT. GFP-$b^{0,+}$AT/BAT1 and GFP-P482L fusion proteins were sorted to the apical membrane of the MDCK II cells when coexpressed with rBAT. In contrast, GFP-$b^{0,+}$AT/BAT1 fusion protein stayed in the cytoplasm when solely expressed. AP and BL indicate apical and basal sites of MDCK II cells, respectively. (**d**) Cell surface biotinylation analysis of $b^{0,+}$AT/BAT1 and P482L. HEK293 cells were transiently expressed with myc-$b^{0,+}$AT/BAT1 plus rBAT (lane 2), myc-P482L plus rBAT (lane 3), myc-$b^{0,+}$AT/BAT1 alone (lane 4), or myc-P482L alone (lane 5). Single bands of ~41 kDa were observed for myc-$b^{0,+}$AT/BAT1 and myc-P482L coexpressed with rBAT (lane 2 and 3). Green: GFP fluorescence; red: 4,6-diamidino-2-phenylindole fluorescence from nuclei.

compared with wild-type $b^{0,+}$AT/BAT1; however, the magnitude of the decrease was much less than that for P482L. In order to further investigate the effect of the alteration of Pro^{482} to Leu, we constructed mutants in which Pro^{482} is changed to various neutral amino acids with varied bulkiness in their side chains. As shown in Figure 6c, the alteration of Pro^{482} to amino acids with bulky side chains such as leucine, isoleucine, methionine, phenylalanine, and tryptophan severely decreased the [^{14}C]L-cystine transport activity, whereas the change to the amino acids with less-bulky side chains such as glycine, alanine, serine, and valine did not affect the functional activity.

DISCUSSION

In the present study, we examined cystinuria patients from oriental population (40 Japanese and one Korean) and found that mutations of *SLC7A9* gene responsible for the disease of the oriental population are quite different from those reported previously for European, North American, and

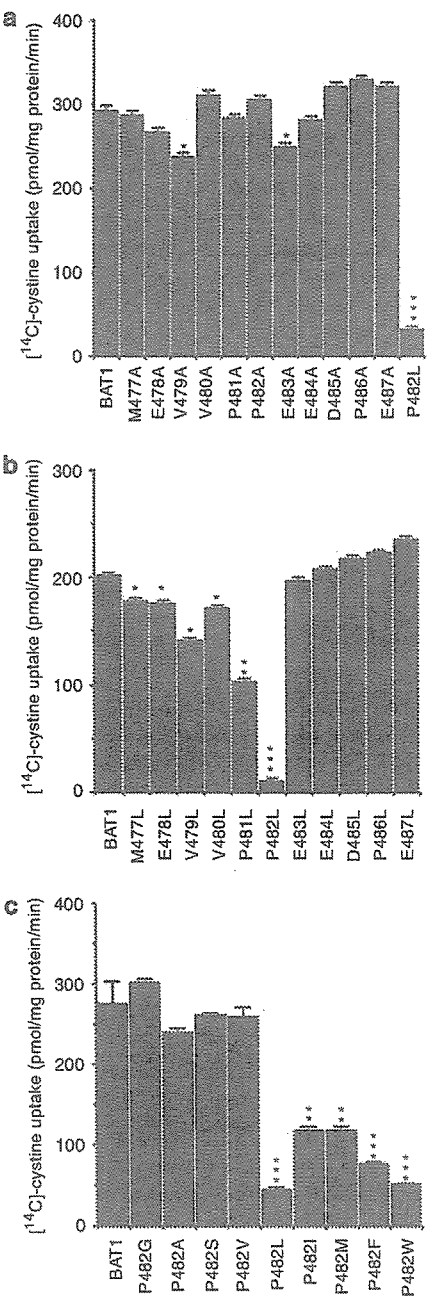

Figure 6 | Effects of site-directed mutagenesis of C-terminus of $b^{0,+}$AT/BAT1 on [^{14}C]L-cystine uptake. (a) The C-terminus amino acids between residues 477 and 487 of $b^{0,+}$AT/BAT1 were systematically mutated to alanine. The site-directed mutants exhibited no remarkable decrease in the uptake of [^{14}C]L-cystine compared with that of wild type except for P482L mutation. (b) The C-terminus amino acids between residues 477 and 487 of $b^{0,+}$AT/BAT1 were systematically mutated to leucine. When Pro^{482} was changed to leucine, the mutants expressed with rBAT exhibited remarkable decrease in the uptake of [^{14}C]L-cystine (100 μM). (c) Pro^{482} of $b^{0,+}$AT/BAT1 was mutated to amino acids with varied bulkiness in their side chains. The alteration of Pro^{482} to leucine, isoleucine, methionine, phenylalanine, and tryptophan remarkably decreased the transport activity, whereas the alteration to glycine, alanine, serine, and valine did not change the transport activity. Asterisks indicate statistical significance ($^{*}P<0.05$; $^{**}P<0.01$; $^{***}P<0.005$, Student's unpaired *t*-test).

Libyan Jewish.[12,16,18] In contrast to W69Stop, G195R, and R333W reported previously,[12,16,18] N227D, R333Q, 1105delA, and P482L found in the present study are novel cystinuria-specific mutations, suggesting that these mutations are unique to Japanese or Asian. It is noted that 31 out of 35 cases with cystinuria-specific mutations examined in the present study involved P482L mutation, whereas this mutation has not been reported for European, North American, and Libyan Jewish population.[12,16,18] It is, therefore, supposed that P482L mutation is prevailing in Japanese and possibly in the other Asian population. G105R, the most frequent mutation for European, North American, and Libyan Jewish population (~25% of non-type I cystinuria cases),[18] was not found in the present study. It is interesting that two cystinuria-specific missense mutations R333Q and R333W found in the present study affect the same amino acid residue, in which R333Q was only found for Japanese cases. Arg^{333} is located in the putative intracellular loop between TM domains 8 and 9 and conserved for human members of heterodimeric amino acid transporter family.[18] It is, thus, proposed that this amino acid residue is critical in the transport function or in the structural framework for the light chains of heterodimeric amino acid transporters.

For P482L mutation most abundantly found in the present study, we examined two family pedigrees and confirmed Mendelian inheritance and phenotype–genotype correlation (Figure 3 and Table 5). The homozygotes of this mutation exhibited severe cystinuria phenotype with episodes of excretion or removal of renal stones and high level of urinary excretion of cystine and dibasic amino acids. Compared with normal individuals, P482L heterozygotes exhibited a higher level of excretion of cystine and dibasic amino acids into urine, consistent with the characteristics of non-type I cystinuria (Table 5). Relatively large range of variation in the amount of urinary excretion was observed among heterozygotes (2-1, 2-2, and 2-7). This might be due to the possible genetic alterations of $b^{0,+}$AT/BAT1 or rBAT that could not be detected in the present study, variations in other factors related to the transporter systems, or differences in diet and metabolism. We found three P482L heterozygotes who suffer from nephrolithiasis. For these patients, no mutation was found in the exons of *SLC3A1* gene encoding rBAT. Although we cannot exclude the involvement of additional mutations of *cis*-regulatory elements of *SLC7A9* gene and *SLC3A1* gene or the mutations of unidentified genes that might be essential for cystine transport, P482L heterozygous mutation could possibly cause cystinuria symptoms dependent on the condition of the patients, which has been reported for classic type II cystinuria with severe phenotypes.[16,20]

P482L is the missense mutation affecting the C-terminus of $b^{0,+}$AT/BAT1. As shown in Figure 2, this mutation results in the loss of function of $b^{0,+}$AT/BAT1 protein coexpressed with rBAT in COS-7 cells, indicating that Pro^{482} plays pivotal role in the functional expression of the transporter. Loss of function of P482L mutant is supposed not due to the loss of protein expression or lack of ability to be sorted to the apical membrane based on the following reasons: first, the anti-myc antibody recognized the band for myc-tagged P482L with the intensity similar to that of wild-type $b^{0,+}$AT/BAT1 (Figure 4b); second, the GFP-tagged P482L protein was sorted to the apical membrane when coexpressed with rBAT in MDCK II cells similar to GFP-tagged wild-type $b^{0,+}$AT/BAT1 (Figure 5b and c); finally, surface biotinylation study revealed that P482L protein as well as wild-type $b^{0,+}$AT/BAT1 protein was detected at the plasma membrane upon coexpression with rBAT in HEK293 cells (Figure 5d). In Figure 4b, the protein products of W69stop and del1105A were not detected. This might be due to the rapid degradation of the immature proteins. A recent study on the crystal structure of *Escherichia coli* 12-membrane-spanning transporters indicated that the substrate binding sites are located in the hydrophilic pocket surrounded by TM helices, suggesting that their N- and C-terminal intracellular domains are not directly involved in the substrate binding and translocation of substrates.[21,22] Mammalian 12-membrane-spanning transporters phylogenetically related to the bacterial 12-membrane-spanning transporters are supposed to possess the analogous structure and operate based on the similar structural trait.[23] In order to examine the roles of Pro^{482} in the C-terminus intracellular domain of $b^{0,+}$AT/BAT1, we performed site-directed mutagenesis analyses. In the first series of experiments, C-terminus amino-acid residues between Met^{477} and Glu^{487} were systematically changed to alanine. Surprisingly, no remarkable decrease was observed in the cystine transport activity even when Pro^{482} was changed to alanine in spite of the severe decrease in the function for Pro^{482}-to-Leu alteration. This indicates that Pro^{482} itself is not essential for the function of $b^{0,+}$AT/BAT1 protein but the incorporation of leucine residue at position 482 interferes with the functional expression.

We, thus, generated additional site-directed mutants in which Pro^{482} was changed to various neutral amino acids. As shown in Figure 6, the alteration of Pro^{482} to amino acids with bulky side chains affected the function of $b^{0,+}$AT/BAT1, whereas the changes to residues with less bulky side chains did not reduce the functional activity. It is, thus, suggested that the bulky side chains incorporated at the C-terminus of $b^{0,+}$AT/BAT1 interfered with the functional expression of $b^{0,+}$AT/BAT1. By examining the site-directed mutants in which residues between Met^{477} and Glu^{487} were systematically changed to leucine, it was found that leucine alteration affected the function of $b^{0,+}$AT/BAT1 only when quite restricted residues were changed to leucine. Based on these observations, we, thus, propose that the bulky side chain incorporated at the position 482 of $b^{0,+}$AT/BAT1 somehow suppressed the transport function possibly by interfering with intra- or intermolecular interactions. The further investigation would lead to the understanding of the novel regulatory mechanisms of heterodimeric amino acid transporters as well as the role of P482L mutation in the pathogenesis of cystinuria.

In the present study, we have identified several novel mutations of *SLC7A9* from oriental population and found that mutations are quite different from those reported previously for European, North American, and Libyan Jewish. Our results contribute toward understanding the distribution and frequencies of cystinuria-related mutations of *SLC7A9*.

MATERIALS AND METHODS

Subjects

Forty-one cystinuria patients (40 Japanese and one Korean) from 39 independent families were studied. All had an episode of delivery or removal of cystine stones. Urinary excretion of cystine and dibasic amino acids was determined in 24 h urine samples by quantitative ion-exchange chromatography or reverse-phase high-performance liquid chromatography. The amino acid content was corrected per gram of creatinine. In all patients whose urinary cystine excretion was analyzed quantitatively, cystine excretion was over 800 nmol/mg creatinine. Urinary hyperexcretion of dibasic amino acids was also confirmed. The urinary excretion of other neutral amino acids was within normal ranges for all patients. For the patients whose urinary amino acid levels were not quantitatively analyzed, the urinary cystine excretion was confirmed by cyanide-nitroprusside test and their cystine stones were analyzed by infrared spectrophotometry.[3] Genomic DNA was obtained from the patients and the members of the selected family pedigrees. Genomic DNA was also obtained from 50 unrelated normal individuals who served as controls. The study protocol was approved by the Institutional Research Boards of Chiba University Graduate School of Medicine and of Kyorin University School of Medicine. All study subjects gave written informed consent, and the ethics committee of Chiba University Graduate School of Medicine and of Kyorin University School of Medicine gave permission for the analyses in relation to cystinuria.

Determination of *exon–intron* boundaries of *SLC7A9*

The location and sequence of all exon–intron boundaries were determined by direct sequencing of the products obtained by PCR amplification of genomic DNA with randomly designed cDNA-derived oligonucleotide primers, using an ABI PRISM Sequencer (Perkin Elmer, Wellesley, MA, USA). *SLC7A9* consisted of 13 exons. The codon for the translation-initiator methionine (ATG) was located in exon 2, whereas the termination codon TAA was located in exon 13. The exon–intron boundaries we determined have turned out to be identical to those obtained by deducing the recently released genomic DNA sequence of *SLC7A9* (accession no. AC008805).[18]

Mutation analysis and direct sequencing

Genomic DNA was extracted from whole blood using the Wizard Genomic DNA Purification Kit (Promega, Madison, WI, USA). Twelve pairs of oligonucleotide primers (Table 1) were synthesized in order to amplify all exons of *SLC7A9* gene by PCR for direct sequencing. In all cases, sequencing of both strands of the PCR products was performed.[24] Mutation analysis of *SLC3A1* gene was performed for the above-described 41 cystinuria patients using oligonucleotide primers as described elsewhere.[25]

Construction of mutant cDNAs

All cDNA mutants were constructed by using the QuikChange site-directed mutagenesis kit (Stratagene, La Jolla, CA, USA) according to the manufacturer's instructions. The mutagenic oligonucleotide primers are shown in Table 2. Proper construction of the mutated cDNAs was confirmed by complete sequencing.

Functional expression in COS-7 cells

cDNAs for human rBAT and those for wild-type or mutated human $b^{0,+}$AT/BAT1 in pcDNA3.1(+) were expressed transiently in COS-7 cells using LipofectAMINE™2000 (Invitrogen, Carlsbad, CA, USA) following the manufacturer's instructions.[26] For co-transfection, 10 μg of cDNA for $b^{0,+}$AT/BAT1 or its mutants and 10 μg of rBAT cDNA were diluted into 1 ml of opti-MEM reduced-serum medium (Invitrogen, Carlsbad, CA, USA) and mixed with 60 μl LF2000 reagent diluted in 1 ml opti-MEM reduced-serum medium. After incubation for 20 min at room temperature, the mixture was applied to COS-7 cells maintained in a tissue culture dish (90 mm diameter) with 70–90% confluence. At 24 h after transfection, the transfected cells were collected and seeded on a 24-well plate (2×10^5 cells/well) in fresh medium. Amino acid uptake measurements were performed at 48 h after transfection of the plasmids as described elsewhere.[26]

Anti-human $b^{0,+}$AT/BAT1 antibodies

Oligopeptides (QMLMEVVPPEEDPEC) corresponding to amino acid residues 474–487 of human $b^{0,+}$AT/BAT1 were synthesized. Anti-peptide antibody was produced as described elsewhere.[27,28]

Construction of the fusion proteins

The fusion proteins in which myc and GFP epitopes were fused to the N-terminus of wild-type and mutant $b^{0,+}$AT/BAT1 were generated. The coding regions of cDNAs for the wild-type and mutant $b^{0,+}$AT/BAT1 were amplified by PCR using primers containing restriction enzyme cleavage sites for *Hin*dIII, *Xho*I, *Eco*RI, or *Kpn*I. After digestion with *Hin*dIII and *Xho*I or *Eco*RI and *Kpn*I, the fragments were ligated with pCMV-Taq3 vector (Stratagene, La Jolla, CA, USA) digested with *Hin*dIII and *Xho*I or pEGFP C2 vector (Clontech, Mountain View, CA, USA) digested with *Eco*RI and *Kpn*I, respectively. Proper construction was confirmed by DNA sequencing.

Western blotting

COS-7 cells were co-transfected with cDNAs for human rBAT and those for wild-type, mutated human $b^{0,+}$AT/BAT1 or their myc-tagged products as described above. At 48 h after transfection, the transfected cells were collected and homogenized as described elsewhere.[29] The anti-human $b^{0,+}$AT/BAT1 (1:2000) antibody or anti-myc (1:2000) antibody (Invitrogen, Carlsbad, CA, USA) was used as the primary antibody. To verify the specificity of immunoreactions by absorption experiments, the membranes were treated with primary antibodies in the presence of antigen peptides (50 μg/ml).[29]

Confocal laser-scanning microscopy

MDCK II cells provided by Dr Dietrich Keppler (European Molecular Biology Laboratory, Heidelberg, Germany) were cultured as described.[30] For localization of $b^{0,+}$AT/BAT1 and P482L mutant protein, MDCK II cells were grown on transwell membranes (membrane diameter 24 mm, pore size 3.0 μm; Costar, Corning, NY, USA) for 1 week (100% confluence) and then co-transfected with cDNAs for myc-tagged human rBAT (1 μg) and those for GFP-tagged wild-type human $b^{0,+}$AT/BAT1 or GFP-P482L (1 μg) using LipofectAMINE™2000. Cells were fixed with 4% paraformaldehyde in phosphate-buffered saline and permeabilized with 0.5% Triton X-100 in phosphate-buffered saline containing 5% goat serum.

Membranes were incubated with an anti-myc (1:500) antibody (Invitrogen, Carlsbad, CA, USA) at room temperature for 1 h. After three washes with phosphate-buffered saline, the membranes were incubated with Alexa Fluor 546 goat anti-mouse IgG (Molecular Probes, Eugene, OR, USA) as a secondary antibody for 1 h. Argon and HeNe laser beams were used for excitation at 488 nm for GFP and 543 nm for Alexa Fluor 546 visualization, respectively. Nuclei were stained with 4,6-diamidino-2-phenylindole nucleic acid staining for 10 min and visualized by excitation at 405 nm with Diode 405 laser. Images were acquired using Carl Zeiss LSM510 META laser-scanning confocal microscope (Carl Zeiss, Frankfurt, Germany).

Cell surface biotinylation

Surface biotinylation of $b^{0,+}$AT/BAT1 and P482L mutant at the plasma membrane of HEK293 cells was performed as describe elsewhere.[31,32] myc-tagged $b^{0,+}$AT/BAT1 and myc-P482L were detected with an anti-myc (1:2000) antibody (Invitrogen) and horseradish peroxidase-conjugated anti-mouse IgG as a secondary antibody (Jackson ImmunoResearch, West Grove, PA, USA).

Statistical analysis

Data are expressed as mean$\pm$s.e.m. Statistical differences were determined using Student's unpaired *t*-test. Mann–Whitney *U*-test was used to analyze urinary amino-acid levels among different genotypes. Differences were considered significant at the level of $P<0.05$.

ACKNOWLEDGMENTS

This work was supported in part by grants from the Ministry of Education, Culture, Sports, Science and Technology of Japan, the Japan Society for the Promotion of Science, the Promotion and Mutual Aid Corporation for Private Schools of Japan, the Japan Health Sciences Foundation, Uehara Memorial Foundation, YASUDA Medical Research Foundation, Heiwa Nakajima Foundation, and Health and Labor Sciences Research Grants for Research on Advanced Medical Technology: Toxicogenomics Project. AC is a research fellow of the Japan Society for Promotion of Science. We thank Dr K Nozumi, Dr T Yoshida, Dr T Igarashi, Dr K Yamaguchi, Dr H Suniya, Dr K Nagashima, Dr M Masai, Dr H Nakatsu, Dr S Tomioka, Dr K Mikami, Dr Y Naya, and Dr K Egoshi for help with obtaining blood samples. We also thank Michi Takahashi, Akie Toki, and Keiko Sakama for technical assistance. Anti-$b^{0,+}$AT/BAT1 antibody was supplied by Kumamoto Immunochemical Laboratory, Transgenic Inc., Kumamoto, Japan.

REFERENCES

1. McKusick VA. Cystiuria. In: *Mendelian Inheritance in Man: Catalog of Autosomal Dominant, Autosomal Recessive, and X-linked Phenotypes*, 9th edn. Johns Hopkins University Press: Baltimore and London, 1990, pp 1128–1129.
2. Segal S, Thier SO. Cystiuria. In: Seriver CR, Beaudet AL, Sly WS, Valle D (eds). *The Molecular and Metabolic Basis of Inherited Disease*. McGraw-Hill: New York, 1995, pp 3581–3601.
3. Ito H, Murakami M, Miyauchi T *et al.* The incidence of cystinuria in Japan. *J Urol* 1982; **129**: 1012–1014.
4. Akakura K, Egoshi K, Ueda T *et al.* The long-term outcome of cystinuria in Japan. *Urol Int* 1998; **61**: 86–89.
5. Rosenberg L, Downing S, Durant J, Segal S. Cystinuria biochemical evidence of three genetically distinct diseases. *J Clin Invest* 1966; **45**: 365–371.
6. Wells RG, Hediger MA. Cloning of a rat kidney cDNA that stimulates dibasic and neutral amino acid transport and has sequence similarity to glucosidases. *Proc Natl Acad Sci USA* 1992; **89**: 5596–5600.
7. Bertran J, Werner A, Moore ML *et al.* Expression cloning of a cDNA from rabbit kidney cortex that induces a single transport system for cystine and dibasic and neutral amino acids. *Proc Natl Acad Sci USA* 1992; **89**: 5601–5605.
8. Tate SS, Yan N, Udenfriend S. Expression cloning of a Na^+-independent neutral amino acid transporter from rat kidney. *Proc Natl Acad Sci USA* 1992; **89**: 1–5.
9. Lee WS, Wells RG, Sabbag RV *et al.* Cloning and chromosomal localization of a human kidney cDNA involved in cystine, dibasic and neutral amino acid transport. *J Clin Invest* 1993; **91**: 1959–1963.
10. Bertran J, Werner A, Chillaron J *et al.* Expression cloning of a human renal cDNA that induces high affinity transport of L-cystine shared with dibasic amino acids in *Xenopus* oocytes. *J Biol Chem* 1993; **268**: 14842–14849.
11. Chairoungdua A, Segawa H, Kim JY *et al.* Identification of an amino acid transporter associated with the cystinuria-related type II membrane glycoprotein. *J Biol Chem* 1999; **274**: 28845–28848.
12. International Cystinuria Consortium. Non-type I cystinuria caused by mutations in *SLC7A9*, encoding a subunit ($b^{0,+}$AT) of rBAT. *Nat Genet* 1999; **23**: 52–57.
13. Pfeiffer R, Loffing J, Rossier G *et al.* Luminal heterodimeric amino acid transporter defective in cystinuria. *Mol Biol Cell* 1999; **10**: 4135–4147.
14. Palacin M, Fernandez E, Chillaron J, Zorzano A. The amino acid transport system $b^{0,+}$ and cystinuria. *Mol Membr Biol* 2001; **18**: 21–26.
15. Palacin M, Borsani G, Sebastio G. The molecular bases of cystinuria and lysinuric protein intolerance. *Curr Opin Genet Dev* 2001; **11**: 328–335.
16. Leclerc D, Boutros M, Suh D *et al.* SLC7A9 mutations in all three cystinuria subtypes. *Kidney Int* 2002; **62**: 1550–1559.
17. Dello Strologo L, Pras E, Pontesilli C *et al.* Comparison between *SLC3A1* and *SLC7A9* cystinuria patients and carriers: a need for a new classification. *J Am Soc Nephrol* 2002; **13**: 2547–2553.
18. Font MA, Feliubadalo L, Estivill X *et al.* Functional analysis of mutations in *SLC7A9*, and genotype–phenotype correlation in non-Type I cystinuria. *Hum Mol Genet* 2001; **10**: 305–316.
19. Calonge MJ, Gasparini P, Chillaron J *et al.* Cystinuria caused by mutations in rBAT gene involved in the transport of cystine. *Nat Genet* 1994; **6**: 420–425.
20. Goodyer P, Saadi I, Ong P *et al.* Cystinuria subtype and the risk of nephrolithiasis. *Kidney Int* 1998; **54**: 56–61.
21. Abramson J, Smirnova I, Kasho V *et al.* Structure and mechanism of the lactose permease of *Escherichia coli*. *Science* 2003; **301**: 610–615.
22. Huang Y, Lemieux MJ, Song J *et al.* Structure and mechanism of the glycerol-3-phosphate transporter from *Escherichia coli*. *Science* 2003; **301**: 616–620.
23. Locher KP, Bass RB, Rees DC. Structural biology. Breaching the barrier. *Science* 2003; **301**: 603–604.
24. Enomoto A, Kimura H, Chairoungdua A *et al.* Molecular identification of a renal urate anion exchanger that regulates blood urate levels. *Nature* 2002; **417**: 447–452.
25. Egoshi K, Akakura K, Kodama T, Ito H. Identification of five novel *SLC3A1* (rBAT) gene mutations in Japanese cystinuria. *Kidney Int* 2000; **57**: 25–32.
26. Mizoguchi K, Cha SH, Chairoungdua A *et al.* Human cystinuria-related transporter: localization and functional characterization. *Kidney Int* 2001; **59**: 1821–1833.
27. Altman A, Cardenas JM, Houghten RA *et al.* Antibodies of predetermined specificity against chemically synthesized peptides of human interleukin 2. *Proc Natl Acad Sci USA* 1984; **81**: 2176–2180.
28. Hisano S, Haga H, Miyamoto K *et al.* The basic amino acid transporter (rBAT)-like immunoreactivity in paraventricular and supraoptic magnocellular neurons of the rat hypothalamus. *Brain Res* 1996; **710**: 299–302.
29. Yanagida O, Kanai Y, Chairoungdua A *et al.* Human L-type amino acid transporter 1 (LAT1): characterization of function and expression in tumor cell lines. *Biochim Biophys Acta* 2001; **1514**: 291–302.
30. Cui Y, Konig J, Buchholz JK *et al.* Drug resistance and ATP-dependent conjugate transport mediated by the apical multidrug resistance protein, MRP2, permanently expressed in human and canine cells. *Mol Pharmacol* 1999; **55**: 929–937.
31. Anzai N, Miyazaki H, Noshiro R *et al.* The multivalent PDZ domain-containing protein PDZK1 regulates transport activity of renal urate-anion exchanger URAT1 via its C terminus. *J Biol Chem* 2004; **279**: 45942–45950.
32. Huh KH, Wenthold RJ. Turnover analysis of glutamate receptors identifies a rapidly degraded pool of the *N*-methyl-D-aspartate receptor subunit, NR1, in cultured cerebellar granule cells. *J Biol Chem* 1999; **274**: 151–157.

The PDZ domain protein PDZK1 interacts with human peptide transporter PEPT2 and enhances its transport activity

R Noshiro[1,2,4], N Anzai[1,4], T Sakata[1,2], H Miyazaki[1], T Terada[3], HJ Shin[1], X He[1], D Miura[1], K Inui[3], Y Kanai[1] and H Endou[1,2]

[1]*Department of Pharmacology and Toxicology, Kyorin University School of Medicine, Mitaka, Tokyo, Japan;* [2]*Fuji Biomedix Co. Ltd, Chuo-ku, Tokyo, Japan and* [3]*Department of Pharmacy, Kyoto University Hospital, Sakyo-ku, Kyoto, Japan*

The proton-coupled peptide transporter PEPT2 (*SLC15A2*) mediates the high-affinity low-capacity transport of small peptides as well as various oral peptide-like drugs in the kidney. In contrast to its well-characterized transport properties, there is less information available on its regulatory mechanism, although the interaction of PEPT2 to the PDZ (PSD-95, DgIA, and ZO-1)-domain protein PDZK1 has been preliminarily reported. To examine whether PDZK1 is a physiological partner of PEPT2 in kidneys, we started from a yeast two-hybrid screen of a human kidney cDNA library with the C-terminus of PEPT2 (PEPT2 C-terminus (PEPT2-CT)) as bait. We could identify PDZK1 as one of the positive clones. This interaction requires the PDZ motif of PEPT2-CT detected by a yeast two-hybrid assay, *in vitro* binding assay and co-immunoprecipitation. The binding affinities of second and third PDZ domains of PDZK1 to PEPT2-CT were measured by surface plasmon resonance. Co-immunoprecipitation using human kidney membrane fraction and localization of PEPT2 in renal apical proximal tubules revealed the physiological meaning of this interaction in kidneys. Furthermore, we clarified the mechanism of enhanced glycylsarcosine (Gly-Sar) transport activity in PEPT2-expressing HEK293 cells after the PDZK1 coexpression. This augmentation was accompanied by a significant increase in the V_{max} of Gly-Sar transport via PEPT2 and it was also associated with the increased surface expression level of PEPT2. These results indicate that the PEPT2–PDZK1 interaction thus plays a physiologically important role in both oligopeptide handling as well as peptide-like drug transport in the human kidney.

Kidney International (2006) **70,** 275–282. doi:10.1038/sj.ki.5001522; published online 31 May 2006

KEYWORDS: oligopeptides; oligopeptide transporter; PEPT2; PDZ; PDZK1

Correspondence: *Y Kanai, Department of Pharmacology and Toxicology, Kyorin University School of Medicine, 6-20-2 Shinkawa, Mitaka, Tokyo 181-8611, Japan. E-mail: ykanai@kyorin-u.ac.jp*

[4]These authors contributed equally to this work.

Received 6 August 2005; revised 21 February 2006; accepted 8 March 2006; published online 31 May 2006

Proton-coupled peptide transporters play an important role in the maintenance of nutrition by mediating the transport of di- and tripeptides across the brush border (apical) membranes of the small intestine and kidney. In addition, peptide transporters function as drug transporters for peptide-like drugs, including β-lactam antibiotics and angiotensin converting enzyme inhibitors.[1–3] Two proton-coupled oligopeptide transporters, PEPT1 and PEPT2, have previously been cloned in rabbits,[4–6] rats[7–9] and humans.[10–12] PEPT1 was thus shown to be a high-capacity, low-affinity transporter that is expressed mainly in small intestine and, to smaller extent, in kidneys. It has been shown to play an essential role in the absorption of small peptides arising from the digestion of dietary proteins. In contrast, PEPT2 was found to be a low-capacity, high-affinity transporter that is expressed in the kidneys. In rats, Pept1 and Pept2 are sequentially expressed: Pept1 is located in the early segment and Pept2 is in the late segment of the proximal tubules.[13] In addition, both Pept1 and Pept2 are localized in the apical membranes of renal proximal tubule in rats.[14,15] Although both transporters are expressed in the kidney, PEPT2 is thought to play a dominant role in the conservation of peptide-bound amino acids. Recently, Rubio-Aliaga *et al.*[16] have reported on the impaired renal reabsorption of peptide-bound amino acids in animals lacking Pept2.

Although the transport properties and characteristics of substrate recognition for PEPT2 have been well documented, there is less information available on PEPT2 regulation. Takahashi *et al.*[17] reported a pronounced upregulation of Pept2 mRNA and protein expression in 5/6 nephrectomized rats 2 weeks after surgery and the downregulation of its mRNA 16 weeks after surgery.[18] Wenzel *et al.*[19] demonstrated that the activation of signaling pathways involving protein kinase C changes the kinetic property of pig Pept2 in a renal cell line. Recently, Bravo *et al.*[20] demonstrated a strong inhibitory effect of EGF on the rat Pept2 transport capacity. However, the modulation of the PEPT2 function by its associated protein(s) still remains unclear.

In recent years, several PDZ domain proteins, such as NHERF1/EBP50, NHERF2/E3KARP, and PDZK1, have been identified in kidneys and thus have been suggested to be involved in the stabilization, targeting, and regulation of their binding partner.[21–24] The PDZ (PSD-95, DglA, and ZO-1)-binding domains have been identified in various proteins and they are considered to be modular protein–protein recognition domains that play a role in protein targeting and protein complex assembly.[25–27] This domain binds to proteins containing the tripeptide motif $(S/T)-X-\varnothing$ (X = any residue and $\varnothing$ = a hydrophobic residue) at their C-termini.[27] As Russel *et al.*[28] mentioned, PEPT2 is localized to the apical membrane and has C-terminal amino-acid sequences that match the PDZ-binding motif (T-K-L), in a manner similar to that of other apical organic anion transporters, such as MRP2/4, NPT1, Oatp1, Oat-k1/k2; thus, indicating that PEPT2 most likely binds to certain PDZ domain proteins. We have recently identified that the urate/anion exchanger URAT1, which has a PDZ motif at its C-terminus (T-Q-F), interacts with PDZK1.[29] Interestingly, both URAT1 and PEPT2 are expressed at the apical membrane of renal proximal tubules and they are considered to function in a reabsorptive pathway for endogenous organic anions (urate[30] and oligopeptides,[1–3] respectively). It is likely that these transporters bind to either the same or other PDZ domain protein(s) via its PDZ-motif.

Very recently, Kato *et al.*[31] examined the interaction between xenobiotic transporters including PEPT2, and PDZ proteins including PDZK1. PDZK1, originally identified as a protein that interacts with MAP17, a membrane-associated protein,[32] has been reported to interact with several membrane proteins through its PDZ domain.[33] Using coexpression of PEPT2 C-terminus (PEPT2-CT) and PDZK1 in yeast, a possible interaction was demonstrated in the artificial condition. Because they solely rely on data from *in vitro* binding assays and did not provide any evidence that this interaction truly occurs in proteins expressed from the endogenous tissue, we performed yeast two-hybrid screening against a human kidney cDNA library using PEPT2-CT as bait and thus characterized this interaction in order to identify PDZK1 as a physiological binding partner of PEPT2.

RESULTS

Identification of PDZK1 by yeast two-hybrid library screening

In an attempt to isolate PEPT2-interacting protein(s) from the endogenous genes, we performed yeast two-hybrid screening against a cDNA library constructed from the human adult kidney using the PEPT2-CT as bait. From the 8.7×10^6 transformants screened, we obtained 64 positive clones. One of these clones had a sequence identical to a portion of the human PDZK1 gene.[32] We could not detect any interactions between PEPT2-CT and any other PDZ proteins that are expressed at and/or beneath the apical membrane of proximal tubules including NHERF1/EBP50, NHERF2/E3KARP, and IKEPP[34–37] (data not shown).

C-terminal PDZ motif of PEPT2 is necessary for PDZK1 interaction

To identify the region of PEPT2 that interacts with PDZK1, we constructed three mutant baits. A bait (PEPT2-CTd3) which lacks the last three residues of PEPT2, which play a crucial role in PDZ domain recognition. Two other baits (L729A and T727A), the extreme C-terminal leucine (0 position) or threonine (−2 position) of PEPT2 was replaced by alanine, which was expected to abolish the PDZ interactions.[38] These three baits did not interact with PDZK1 (Figure 1a). Therefore, the binding through PEPT2-CT suggests that the PDZ motif of PEPT2 is the site of interaction with PDZK1.

The interaction specificity between PDZK1 and PEPT2-CT was confirmed by a yeast two-hybrid assay using a bait that had the C-terminus of another human peptide transporter, PEPT1. PDZK1 did not interact with PEPT1-CT which lacks a PDZ motif (K-Q-M) (Figure 1b).

Interaction of PDZK1 individual PDZ domains with PEPT2-CT

PDZK1 possesses four PDZ domains which facilitate the assembly of protein complexes when target proteins bind via their C-terminal PDZ motifs. To determine the possible interactions of PEPT2-CT with the PDZ domains of PDZK1, we produced prey vectors, with each containing one of the individual PDZ domains (PDZ domain 1 (PDZ1), PDZ2, PDZ3, and PDZ4) from PDZK1. The interaction with the

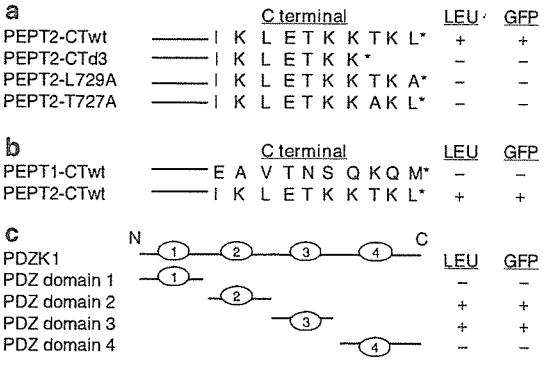

Figure 1 | Specificity of PDZK1 interaction with C-termini of PEPT2 in yeast two-hybrid system. (**a**) PDZK1 specifically interacted with the wt PEPT2 C-terminus but not with the C-terminal mutants L729A, T727A, and d727–729 (d3) of PEPT2. (**b**) Full-length PDZK1 interacting with the intracellular C-terminus of PEPT2 but not with that of PEPT1. (**c**) The wt PEPT2 C-terminus bait interacts with prey containing either the second or third PDZ domains of PDZK1 (PDZ2, PDZ3). The specificity of the prey containing a single PDZ domain of PDZK1 for the PEPT2 bait was confirmed by the absence of growth associated with the PEPT2 d3 mutant baits. The bars represent the approximate length of the baits, and the sequence of the last 10 amino acids is shown. pJG4-5 with PDZK1 cDNA expression cassette is under the control of the GAL1 promoter, such that library proteins are expressed in the presence of galactose (Gal) but not glucose (Glu). The system used for the yeast two-hybrid screen includes the reporter genes LEU2 and GFP, which replace the commonly used classical *lacZ* gene and allow a fast and easy detection of positive clones with long-wave UV. The results from the growth assay and GFP fluorescence are indicated on the right.